Response of vegetation to drought time-scales across global land biomes

Sergio M. Vicente-Serrano[a,1], Célia Gouveia[b,c], Jesús Julio Camarero[d], Santiago Beguería[e], Ricardo Trigo[b,f], Juan I. López-Moreno[a], César Azorín-Molina[a], Edmond Pasho[a], Jorge Lorenzo-Lacruz[a], Jesús Revuelto[a], Enrique Morán-Tejeda[a], and Arturo Sanchez-Lorenzo[g]

[a]Instituto Pirenaico de Ecología, Consejo Superior de Investigaciones Científicas, 50059 Zaragoza, Spain; [b]Centro de Geofisica Universidad de Lisboa, Instituto Dom Luiz, Faculdade de Ciências, Universidade de Lisboa, 1749-016 Lisbon, Portugal; [c]Escola Superior de Tecnologia, Instituto Politécnico de Setúbal, 2910-761 Setúbal, Portugal; [d]Fundación Agencia Aragonesa para la Investigación y Desarrollo–Instituto Pirenaico de Ecología, Consejo Superior de Investigaciones Científicas, 50059 Zaragoza, Spain; [e]Estación Experimental de Aula Dei, Consejo Superior de Investigaciones Científicas, 50059 Zaragoza, Spain; [f]Departamento de Engenharias, Universidade Lusófona, 1749-024 Lisboa, Portugal; and [g]Institute for Atmospheric and Climate Science, Eidgenössische Technische Hochschule Zurich, 8006 Zurich, Switzerland

Edited by Robert E. Dickinson, The University of Texas at Austin, Austin, TX, and approved November 27, 2012 (received for review April 27, 2012)

We evaluated the response of the Earth land biomes to drought by correlating a drought index with three global indicators of vegetation activity and growth: vegetation indices from satellite imagery, tree-ring growth series, and Aboveground Net Primary Production (ANPP) records. Arid and humid biomes are both affected by drought, and we suggest that the persistence of the water deficit (i.e., the drought time-scale) could be playing a key role in determining the sensitivity of land biomes to drought. We found that arid biomes respond to drought at short time-scales; that is, there is a rapid vegetation reaction as soon as water deficits below normal conditions occur. This may be due to the fact that plant species of arid regions have mechanisms allowing them to rapidly adapt to changing water availability. Humid biomes also respond to drought at short time-scales, but in this case the physiological mechanisms likely differ from those operating in arid biomes, as plants usually have a poor adaptability to water shortage. On the contrary, semiarid and subhumid biomes respond to drought at long time-scales, probably because plants are able to withstand water deficits, but they lack the rapid response of arid biomes to drought. These results are consistent among three vegetation parameters analyzed and across different land biomes, showing that the response of vegetation to drought depends on characteristic drought time-scales for each biome. Understanding the dominant time-scales at which drought most influences vegetation might help assessing the resistance and resilience of vegetation and improving our knowledge of vegetation vulnerability to climate change.

drought impacts | NDVI | drought adaptation | Standardized Precipitation Evapotranspiration Index | drought index

Drought is a natural phenomenon that occurs when water availability is significantly below normal levels over a long period and the supply cannot meet the existing demand. Drought is one of the main drivers of the reduction in Aboveground Net Primary Production (ANPP) (1), although land ecosystems differ in their sensitivity to drought (2). However, a general theory of the effects of drought on land vegetation is lacking and the subject of scientific debate (2–4).

Understanding the response of land vegetation to drought is a crucial challenge, as growth and CO_2 uptake by plants are constrained to a large extent by drought (5). Its study is hindered by difficulties for drought quantification (6) and by the synergistic effects of temperature rise and drought on vegetation (7, 8). Differences in the physiological response of plant species to drought determine different levels of resistance and resilience to water deficits (9, 10) and ultimately influence the type of impact of a drought, differentiating those that slow growth (11) or reduce greenness (12), those that lead to loss of biomass (5), and those that result in plant mortality (8, 13).

The quantification of drought is a difficult task, as we usually identify a drought by its effects on different systems (agriculture, water resources, ecosystem), but there is not a unique physical variable we can measure to quantify drought intensity. Droughts are difficult to pinpoint in time and space, and it is very difficult to quantify their duration, magnitude, and spatial extent with a single variable or metric. Furthermore, the intrinsic multiscalar nature of drought introduces another element of uncertainty. In recent years the concept of drought time-scale has been widely used in drought studies (6, 14). The term refers to the time lag that typically exists between the starting of a water shortage and the identification of its consequences, for example by a decrease of the ANPP or an increase of tree mortality. Thus, the time-scales at which different plant species respond to drought may differ noticeably (11, 12, 15).

The response to water deficit among vegetation types is a crucial issue underlying geographic patterns of vegetation and a central concept to understanding the structure and dynamic of terrestrial ecosystems (2, 16). Nevertheless, the way by which the temporal variability of drought determines vegetation activity across the world biomes remains largely unknown because vegetation types have different characteristic response times (11, 15) and vulnerability (9, 10) to drought. Moreover, most studies considered the response of vegetation to climate by means of the simple anomaly of precipitation with respect to the average conditions. Such approach neglects the role of temperature and the drought time-scale at which the response of vegetation is highest. Both elements are essential to identify the response to climate variability and to understand the sensitivity of vegetation to drought.

In this study we focus on the analysis of drought impacts on vegetation by means of three vegetation parameters: (*i*) vegetation activity and greenness, (*ii*) tree radial growth, and (*iii*) ANPP. We stress the importance of considering the drought time-scale to understand drought impacts on a variety of vegetation types and biomes. For this purpose, we used the Standardized Precipitation Evapotranspiration Index (SPEI) (17), which is a site-specific drought indicator of deviations from the average water balance (precipitation minus potential evapotranspiration) (*SI Appendix*). Different SPEIs are obtained for different time-scales representing the cumulative water balance over the previous n months. The SPEI includes the role of temperature on drought severity by means of its influence on the atmospheric evaporative demand, hence improving the performance of previous drought indices based on precipitation data alone when determining the drought impacts on different hydrological and ecological systems (6, 18).

Results and Discussion

Considering an annual summary of the analysis of the Global Inventory Modeling and Mapping Studies–Normalized Difference Vegetation Index (GIMMS-NDVI) dataset, the vegetation activity

Author contributions: S.M.V.-S., C.G., S.B., R.T., and J.I.L.-M. designed research; S.M.V.-S., J.J.C., and S.B. performed research; S.M.V.-S., C.G., J.J.C., S.B., C.A.-M., E.P., J.L.-L., J.R., E.M.-T., and A.S.-L. analyzed data; and S.M.V.-S., J.J.C., S.B., R.T., and J.I.L.-M. wrote the paper.

The authors declare no conflict of interest.

This article is a PNAS Direct Submission.

[1]To whom correspondence should be addressed. E-mail: svicen@ipe.csic.es.

This article contains supporting information online at www.pnas.org/lookup/suppl/doi:10.1073/pnas.1207068110/-/DCSupplemental.

correlates with drought in large areas of the world (Fig. 1*A*), although drought influence on NDVI changed markedly with season and among regions (*SI Appendix*, Figs. S1 and S2). Correlation between the SPEI and the GIMMS-NDVI data are particularly strong throughout large regions (e.g., eastern North America, the Mediterranean Basin, the Sahel). Overall, 72% of the vegetated land areas show significant correlation between the GIMMS-NDVI and the SPEI (*SI Appendix*, Fig. S3 and Table S2).

Tree-ring width data come predominantly from sites corresponding to mountain areas, temperate regions, and high latitudes of the Northern Hemisphere. Therefore, several forest types are not sampled, mainly in tropical and subtropical areas in which tree growth is not subject to seasonal variation and tree-rings are rarely formed, thereby limiting global spatial comparisons. Nevertheless, the high density of tree-ring series in North America, covering humid (mean annual water balance higher than 500 mm per year), subhumid (between 0 and 500 mm), semiarid (between 0 and –500 mm), and arid (lower than –500 mm) sites, shows that forests located in the semiarid and arid areas of central and southwest United States and Mexico have the highest correlations between the SPEI and tree-ring width (*SI Appendix*, Fig. S4). The same pattern is observed with the NDVI and the ANPP datasets, as the influence of the SPEI is lower in humid regions (including tropical rainforests and cool temperate areas of the northern hemisphere) than in semiarid and arid ones (*SI Appendix*, Fig. S5). This is consistent with other studies based on ANPP data (2, 19), as humid regions are characterized by a positive water balance and by vegetation having low water use efficiency (16, 19). Nevertheless, although vegetation activity in humid areas is less determined by drought than in arid ones, drought events also cause a marked reduction of vegetation activity and ANPP (16), as has been observed in the Amazon basin, particularly during the droughts of 2005 (20) and 2010 (21). Accordingly, the GIMMS-NDVI analysis showed that 78% of tropical and subtropical rainforests are

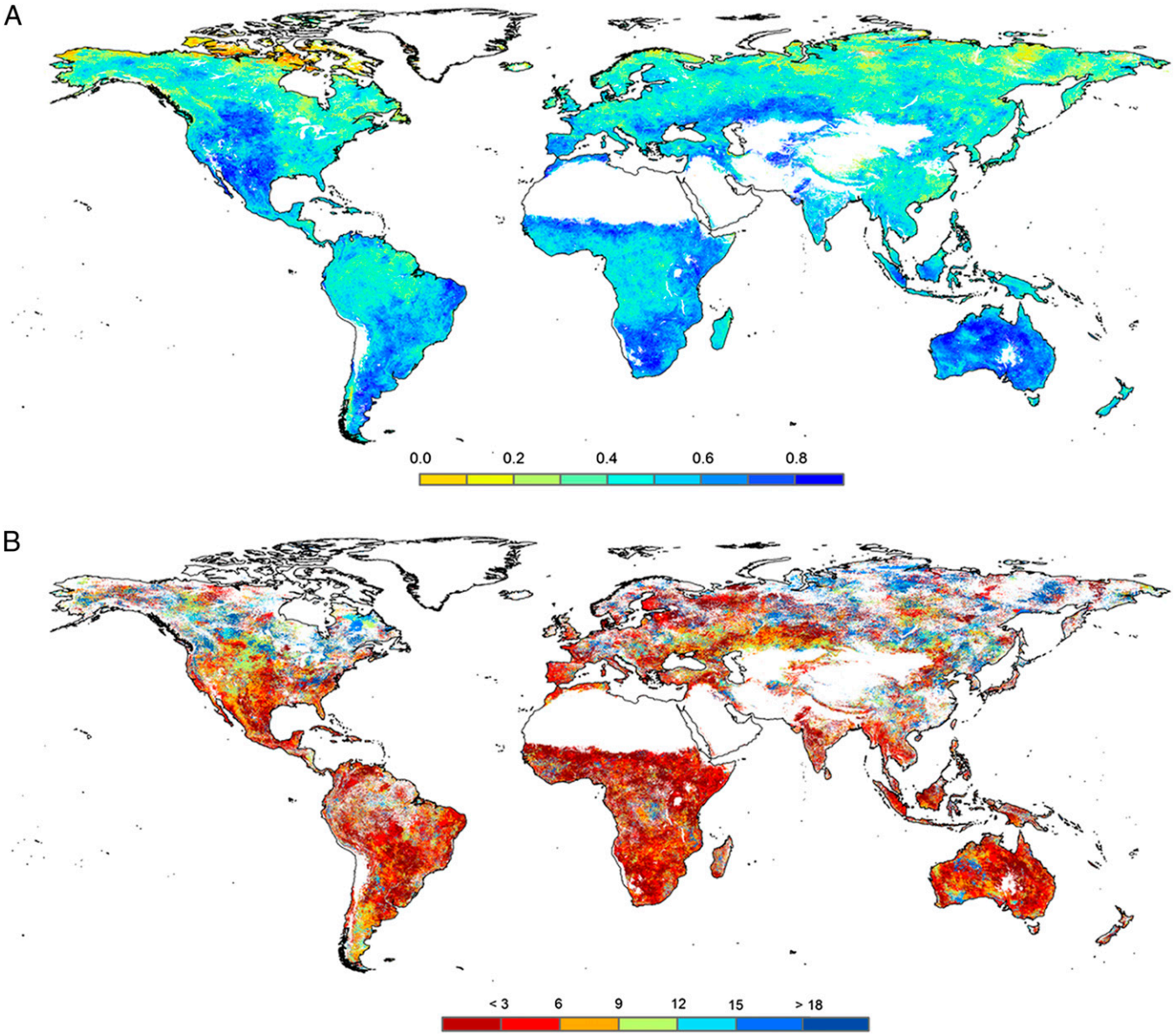

Fig. 1. Geographical patterns of the association observed between drought and vegetation activity. (*A*) Spatial distribution of the correlations (Pearson coefficient, *r*) between SPEI and GIMMS-NDVI for the period 1981–2006. The values represent the maximum correlation recorded for each pixel, independently of the month of the year and the SPEI time-scale. (*B*) SPEI time-scales at which the maximum correlation between SPEI and GIMMS-NDVI is found. Areas with no significant correlations are depicted in white. Desert and ice areas are masked and not included in the analyses.

characterized by significant correlation with the SPEI. This percentage was found to be even higher for the Moderate Resolution Imaging Spectroradiometer (MODIS) images obtained for the period 2001–2009 [90.7% for the Enhanced Vegetation Index (EVI), and 90.9% for the NDVI]. The percentage of surface area showing significant correlations was also high for boreal forests, cool temperate moist forests and rainforests (65.6% for the GIMMS-NDVI, and 85.5% and 84.4% for the MODIS-EVI and MODIS-NDVI datasets, respectively).

One of the main climate drivers of the geographical distribution of vegetation types is the water balance—that is, the difference between the annual precipitation and the atmospheric water demand (22). The water balance determines forest gradients and variations of forest biomass (23), but also the resistance of vegetation to drought explains the spatial distribution of vegetation in both humid (24) and dry environments (25). It is a reasonable hypothesis to think that not only the average water balance but also the characteristics related to the temporal variability (i.e., the frequency, severity, and duration of drought episodes) may play an important role in explaining the spatial distribution of vegetation types. Following the classification of world biomes by Holdridge (*SI Appendix*, Fig. S6), we found a relationship between the mean water balance in each biome and the average influence of droughts on the interannual variability of NDVI (Fig. 2*A*), tree growth (Fig. 2*B*), and ANPP (Fig. 2*C*). The drought influence was quantified by means of correlations between the SPEI series and the series of the three vegetation parameters. Thus, wet and moist forests of each region are always located in areas with a positive water balance, where the control of vegetation activity by drought is low, as indicated by low correlation with the SPEI. In cold regions, where temperature but not precipitation is the major constraint on plant development, there is little influence of drought on vegetation activity, resulting in low correlations too. In temperate, subtropical, and tropical regions, there are clear gradients of drought influence on vegetation activity as a function of the annual water balance, as revealed by large differences in the correlation with the SPEI. These areas contain dry biomes (including dry forests, scrublands, steppes) with very low ANPP (1, 2), which show the highest correlations with the SPEI.

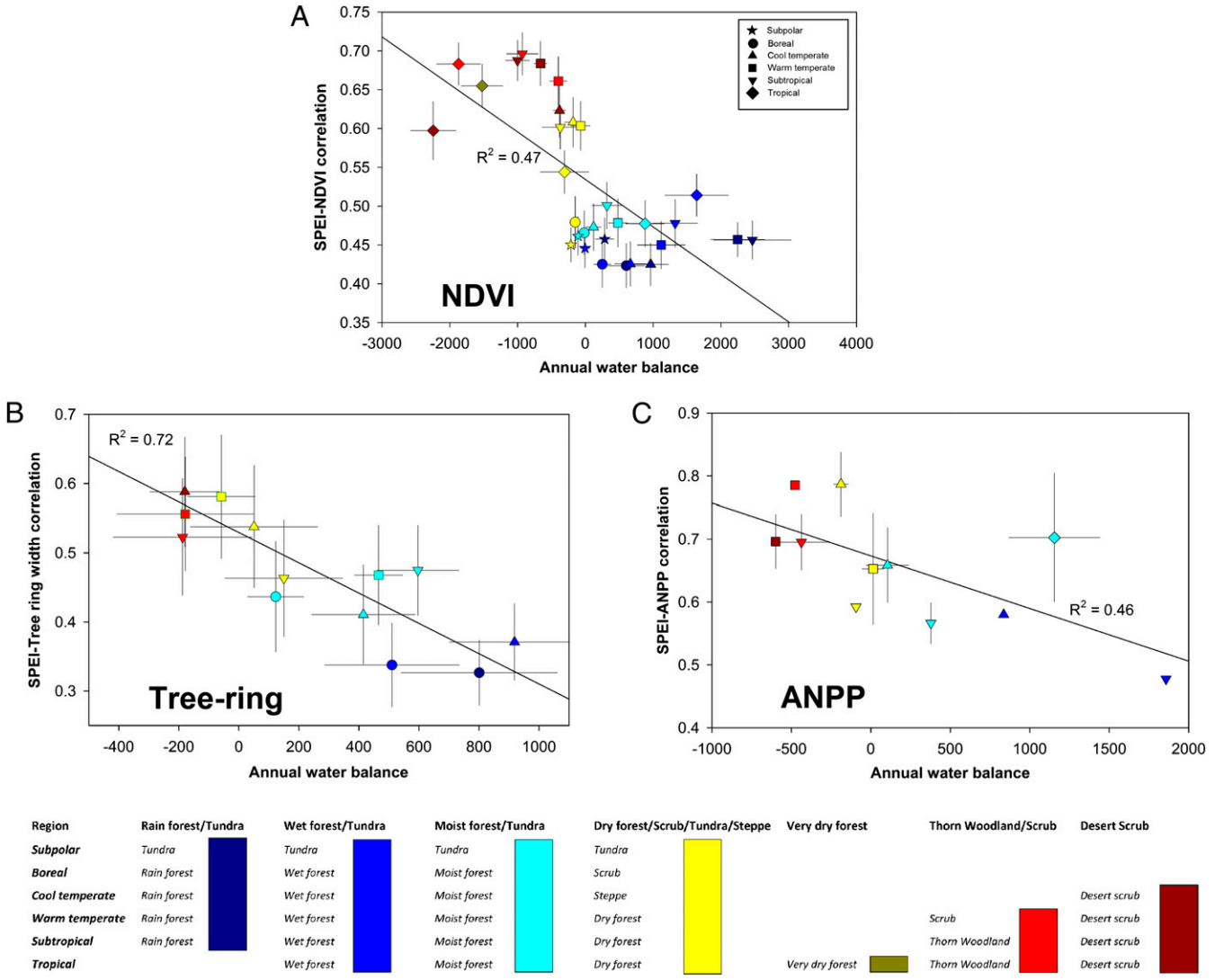

Fig. 2. (*A*) Relationships between the average SPEI/GIMMS-NDVI maximum Pearson correlation coefficients and the average annual water balance (in mm) across the world biomes. (*B*) Relationships between the average SPEI/tree-ring width correlations and the average annual water balance across the world biomes. (*C*) Relationships between the average SPEI/ANPP correlations and the average annual water balance across the world biomes. The biomes are grouped according to six eco-regions: subpolar, boreal, cool temperate, warm temperate, subtropical, and tropical. Colors represent the different biomes of each one of the six eco-regions in the *A*, *B*, and *C* plots. The symbols represent the different eco-regions in plots *A*, *B*, and *C*. Error bars represent ±1/2 SDs. The linear fits and their coefficients of determination are also shown in all graphs.

The time-scales at which droughts affect vegetation provide useful information to understand how biomes respond to drought. From analysis of the SPEI time-scales at which the maximum correlations are recorded, we found that vegetation activity responds predominantly to short drought time-scales (e.g., 2–4 mo; *SI Appendix*, Fig. S7), although spatial variability is high (Fig. 1*B*). Nevertheless, it is possible to identify general patterns, as the NDVI, for example, tends to respond to shorter drought time-scales in arid areas than in humid ones. This pattern is particularly evident in regions that include the most arid biomes. In warm temperate, subtropical, and tropical regions, the most arid biomes tend to respond at shorter time-scales than the humid ones (Fig. 3). This could be related to different mechanisms, which allow plants to reduce the damage caused by water deficits in arid areas (9). Generally, arid ecosystems respond in a highly plastic way to water availability (26), as plant species are adapted to water shortage (27) thanks to physiological, anatomical, and functional strategies that reduce water loss, respiration costs, photosynthetic activity, and growth rate

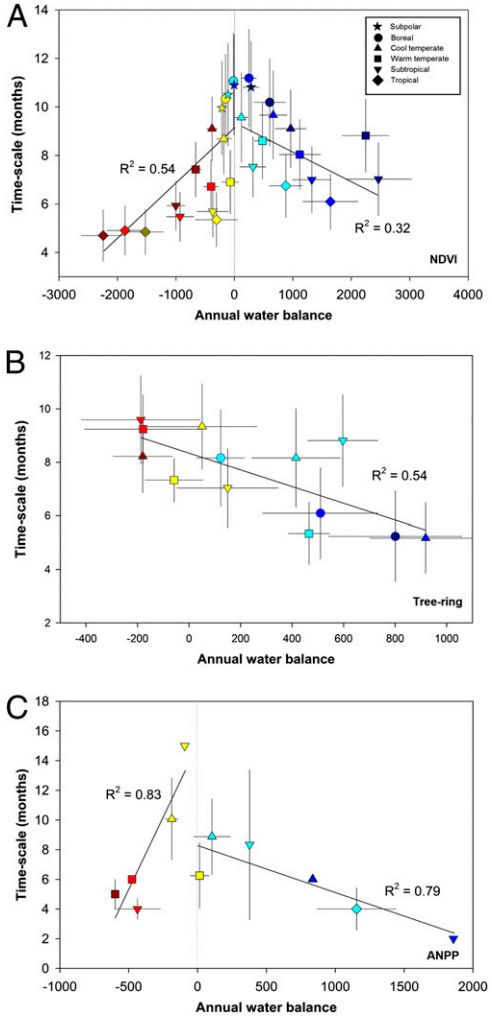

Fig. 3. (*A*) Relationships between the average SPEI time-scales at which the maximum SPEI/GIMMS-NDVI correlation is found and the average annual water balance across eco-regions considering separately negative and positive water balances. (*B*) Relationship between the average SPEI time-scale at which maximum SPEI/tree-ring correlation is found and the average annual water balance across eco-regions. (*C*) Relationship between the average SPEI time-scale at which maximum SPEI/ANPP correlation is found and the average annual water balance across eco-regions for negative and positive water balances. Error bars represent ±1/2 SDs. The linear fits and the coefficients of determination are also shown in all graphs. See corresponding colors in the legend of Fig. 2.

(9). When areas with positive water balance are analyzed independently, it is found that correlations between SPEI and NDVI (Fig. 4*A*, blue), ANPP (Fig. 4*B*, blue), and tree growth (Fig. 4*C*) tend to occur at shorter time-scales as the average water balance increases. This suggests that the influence of drought time-scales is relevant to explain the temporal variability of vegetation parameters also in humid biomes.

In contrast with arid and humid regions, vegetation in semiarid and subhumid regions tends to respond to drought at longer time-scales. Vegetation of these regions is adapted to tolerate regularly periods of water deficit and has physiological mechanisms to cope with these conditions (9). Therefore, it is a reasonable hypothesis to consider that these plant communities must be exposed to sustained water deficits—that is, those registered by long time-scales of the SPEI—to be negatively affected by drought. Thus, in areas with water balance approaching zero, the highest correlations between SPEI and NDVI, tree-ring width, and ANPP occur at time-scales between 8–10 mo, but in the areas with the most positive water balance, the highest correlations between SPEI and vegetation parameters are found at shorter time-scales than in subhumid regions. There are relatively few tree-ring records available for wet tropical rainforests. However, the available data for humid boreal and cool temperate forests show a dominant response to drought at shorter time-scales than is generally recorded for semiarid and subhumid forests (Fig. 3). Boreal and cool temperate moist forests are thus highly sensitive to drought (28), an indicator that tree species dominating these forests do not tolerate water deficits (29). This may explain why droughts predominantly affect tree growth in these areas at short time-scales, as even a short period of water deficit could have negative consequences in vegetation activity and plant growth. Although tree-ring data are not available for the most humid areas of the world such as the tropical rainforests, the results derived from the NDVI suggest a similar pattern: a predominant effect of short-term droughts on vegetation activity (Fig. 3 and *SI Appendix*, Fig. S8). Previous studies identified a lagged response between drought, declining plant growth (30), and forest mortality (31) in similar humid forests. Using various drought time-scales, we have shown that this lag might be usually short, as demonstrated by the response of vegetation activity, forest growth, and the ANPP to very short drought time-scales.

Knowledge of the dominant time-scales at which drought influences vegetation could be critical for the early detection of vegetation damage, but it may also be useful for identifying response patterns that determine the resistance of diverse vegetation types and biomes to drought. Drought vulnerability, however, is related not only to the resistance of vegetation to water stress but also to how fast it recovers after the episode has ended—that is, by its resilience. Drought resilience depends on a variety of factors including the severity and duration of the water deficit, but also the vegetation type (32), the type and magnitude of the damage (33), the plant growth rates and competition between species (34), and even variations in environmental conditions recorded at small spatial scales (35). Although our analysis did not focus on the recovery times of vegetation after drought disturbance, the concept of drought time-scales also seems to constitute a promising tool for analyzing vegetation resilience to drought.

It is noteworthy that the highest influence of drought on vegetation identified in arid areas does not imply necessarily that plant communities from those areas are more vulnerable to drought than those dominant in humid biomes (3, 10). Thus, the short drought time-scales that mostly affect both arid and humid biomes are probably indicative of different types of impacts and different biophysical mechanisms. In arid and semiarid regions, drought impacts usually result in decreased vegetation activity (15) and plant growth (11), but rarely cause plant mortality or long-term damage, as plant communities commonly exhibit a strong resistance to water stress (36), as they contain species that are well adapted to water shortage through different mechanisms (9). This is in agreement with studies analyzing long-term trends of vegetation greenness in arid ecosystems that demonstrated the capacity of such ecosystems to recover the initial greenness values after

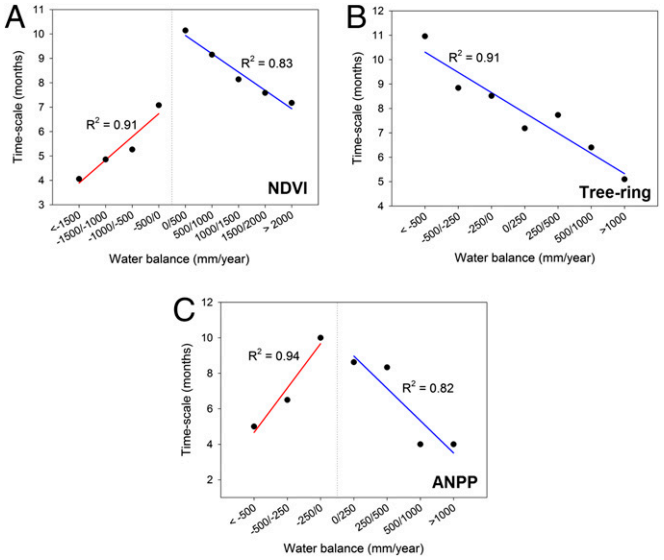

Fig. 4. Average values of the time-scales (in months) at which the GIMMS-NDVI/SPEI (*A*), the tree-ring width/SPEI (*B*), and the ANPP/SPEI (*C*) maximum correlations are recorded, summarized for different ranges of the annual water balance. The linear fits and the corresponding coefficients of determination for negative and positive water balances are also shown.

severe and long-lasting droughts as soon as water is available (37). Nevertheless, although vegetation in arid regions is usually highly resistant to drought (3), when strong damages (e.g., tree mortality) occur during very extreme droughts, the recovery rates after the event has passed may be slow, as arid woody species have generally slow growth rates (38). Thus, unusual severe droughts, which correspond to long SPEI time-scales, can cause plant mortality (34) and even trigger desertification processes (35) in arid environments. Moreover, recurrent droughts can produce a progressive loss of resilience that affects negatively the ability of recovering the initial state (39), often leading to vegetation change.

In general, drought vulnerability is much larger in humid biomes than in arid ones (3, 24), although we found a lower response to drought in the former. This might be explained by the more complex relationship between drought and vegetation activity and plant growth in humid areas because they are characterized by water surplus. Consequently a negative SPEI there does not necessarily imply a water deficit because the water balance may still be positive, albeit lower than usual. Moreover, in humid sites other factors including phenological aspects such as the period of active leaf flushing and vapor pressure deficit may influence the effect of drought on plants (40). In humid regions, drought impacts are most probably linked to damages to plant tissues that result in loss of foliar biomass (29, 31), given the general poor tolerance of plants to water stress (3, 10), but the fast growth rates characteristic of plants of humid regions could allow vegetation to recover its prior state in a short period as soon as the drought has ended. However, in humid areas, long-lasting or recurrent droughts may also be too intense to allow for a fast vegetation recovery, and this could help explain some recent plant mortality episodes in humid forests around the world after severe drought events (7, 20, 29).

Our results concerning the time-scales of drought are similar irrespective of the data sources used: NDVI from National Oceanic and Atmospheric Administration-Advanced Very High Resolution Radiometer and MODIS images, EVI from MODIS images, a vast dataset of tree-ring growth series, and ANPP series across the world. Therefore, our results should be considered robust and unlikely to be explained by alternative causes, such as (*i*) possible residual noise in the GIMMS dataset, (*ii*) the saturation of the NDVI at high values of leaf area index, (*iii*) the low temporal coverage of the MODIS dataset, (*iv*) the low spatial representativeness of the available ANPP series, and (*v*) the lack of adequate coverage of dry and very humid regions by the tree-ring growth dataset. Despite the uncertainties present in each dataset, all of them point toward the same conclusions, and taking into account their complementary nature, this further enhances the robustness of our findings.

Overall, our results provide extensive evaluation of the impact of droughts on global vegetation activity and plant growth. They are particularly relevant within the changing climate framework because the degree to which ecosystems respond to limited water indicates how responsive they may be to future changes in precipitation and temperature. Therefore, the assessment of drought impacts on vegetation parameters may improve the accuracy of projections of vegetation shifts under global change scenarios. Global warming will almost certainly continue in the future (41), which would imply more land areas vulnerable to drought stress, including humid areas such as temperate, mountain, boreal, and wet tropical forests. Vegetation in these areas is already subject to increased drought stress leading to local and regional die-off events because of warming-induced drought stress (7, 29, 31). Although with increased aridity a reduction in vegetation activity might be partially compensated for by rising atmospheric CO_2 concentrations, this mechanism will not enhance production under drought conditions because plant physiological processes are highly constrained by water deficits, independently of the atmospheric CO_2 concentration (42). Increasing drought severity in humid areas may have unpredictable consequences for the biosphere and the global carbon cycle, because the main terrestrial carbon pool is stored in the humid world biomes (43).

In conclusion, we show that vegetation responds to drought at different characteristic time-scales across regions and biomes. Vegetation of both arid and humid biomes respond mostly at short drought time-scales (i.e., a fast reaction of several vegetation parameters is found as soon as relative water deficit occurs), but the mechanisms that drive this response are most likely very different. These mechanisms affect the resistance and resilience of vegetation to drought stress, conditioning their vulnerability to drought. Understanding the relationship between these mechanisms and the characteristics of droughts (for example, as determined by the drought time-scale) is crucial for improving our knowledge of vegetation vulnerability to climate fluctuations and climate change. As expected from current climate change scenarios, the water balance will become more negative in most areas of the world as a consequence of warming processes, which will probably reinforce drought severity worldwide (44).

Methods

To quantify drought severity we used monthly data of the SPEI at a spatial resolution of 0.5° and time-scales ranging from 1 to 24 mo obtained from the SPEIbase (45) (http://sac.csic.es/spei/download.html, *SI Appendix*). We used three different datasets of vegetation parameters, which provide information on ANPP, leaf photosynthetic activity, and tree radial growth across the world. First, we collected long-term ANPP series from the scientific literature using the published tabular data or by digitizing figures. A total set of 40 series that contain a minimum of 10 y were collected (*SI Appendix*, Table S1). The series cover different biomes and vegetation types. The second dataset was based on annual tree-ring width data, obtained from the International Tree-Ring Data Bank (www.ncdc.noaa.gov/paleo/treering.html). From the entire dataset, we selected the tree-ring width series with at least 25 y of data within the period 1945–2009. A total number of 1,846 site chronologies were selected and analyzed (*SI Appendix*). Finally, we included time series of vegetation indices obtained from long-term satellite imagery. We used the NOAA GIMMS-NDVI (46) from July 1981 to December 2006, at a resolution of 0.1°, available from the Global Land Cover Facility (www.glcf.umd.edu/data/gimms). Vegetation indices from the MODIS were also used to replicate the GIMMS-NDVI for the period 2001–2009. Monthly composites of the EVI (47) and the NDVI at a spatial resolution of 5.6 km from the MOD13A2 dataset were obtained from NASA (https://lpdaac.usgs.gov). To characterize the spatial distribution of the world biomes, we used the Holdridge classification (48) from the United Nations Environment Program–Division of Early Warning and Assessment/Global Resource Information Database–Geneva (www.grid.unep.ch) at a spatial resolution of 0.5°. The Global Land Cover Map (http://ionia1.esrin.esa.int/) was used with the purpose of masking the urban areas and irrigated lands.

The 0.5° SPEI data series were interpolated to 8 km for 1981–2006 to match the spatial resolution of the GIMMS-NDVI and to 5.6 km for the

2001–2009 to match the MODIS vegetation indices. The biweekly GIMMS-NDVI series were monthly composited according to the maximum monthly value to avoid different sources of noise. Taking into account the Gaussian shape of the monthly NDVI distributions (49), the 1981–2006 GIMMS-NDVI and the 2001–2009 MODIS EVI and NDVI series were standardized, according to the average and the SDs of the monthly series obtained for each NDVI pixel. In addition, annual ANPP and tree-ring growth series were also standardized before applying the analysis.

The impact of the SPEI interannual variability on vegetation activity, tree growth, and ANPP was assessed by means of parametric correlations using the Pearson coefficient for the entire period of available data, and considering a significance threshold of $\alpha < 0.05$. Twelve series of the GIMMS-NDVI (one per month) were obtained per pixel, and each one was correlated (Pearson coefficient) to the monthly 1- to 24-mo SPEI series of the pixel for the period 1981–2006. For each grid cell, we obtained 288 correlation values (24 for each month of the year). To eliminate the influence of phenology on the results, the monthly correlations were summarized seasonally and annually. For this purpose, the highest correlation found in each season was retained and also the SPEI time-scale at which the maximum seasonal correlation was obtained. After that, seasonal results were summarized annually following the same approach. The same methodology was applied to the MODIS datasets, ANPP, and tree-ring series (*SI Appendix*).

Maximum annual and seasonal correlations between the GIMMS and MODIS vegetation indices and the SPEI as well as maximum annual correlations between tree-ring width and ANPP records and the SPEI were summarized according to the Holdridge classification by means of the calculation of the average correlation and average maximum SPEI time-scale for the different biomes. For this purpose, the average aridity conditions in each biome were quantified using precipitation and potential evapotranspiration data taken from the CRU TS3.0 dataset (*SI Appendix*).

ACKNOWLEDGMENTS. We thank to the two anonymous reviewers for their helpful comments, which have noticeably improved the final manuscript. We also thank the GIMMS and the MODIS science team of the National Aeronautics and Space Administration for providing the remote sensing data. We would also like to thank the Climate Research Unit of the University of East Anglia (United Kingdom) for providing the global land temperature and precipitation dataset used to obtain the SPEIbase and the contributors of the International Tree-Ring Data Bank for providing the tree-ring records used in this study. This work was supported by projects financed by the Spanish Commission of Science and Technology (CGL2011-27574-CO2-02, CGL2011-27536, and CGL2011-26654) and the Aragón Government. C.G. and R.T. were supported by Project PTDC/AAC-CLI/103361/2008 funded by the Portuguese Foundation for Science and Technology. J.J.C. thanks the support of ARAID, and A.S-L. was supported by a post-doctoral fellowship from the Generalitat de Catalunya (2009 BP-A 00035).

1. Webb WL, Lauenroth WK, Szarek SR, Kinerson RS (1983) Primary production and abiotic controls in forests, grasslands, and desert ecosystems in the United States. *Ecology* 64(1):134–151.
2. Knapp AK, Smith MD (2001) Variation among biomes in temporal dynamics of aboveground primary production. *Science* 291(5503):481–484.
3. Maherali H, Pockman WT, Jackson RB (2004) Adaptative variation in the vulnerability of woody plants to xylem cavitation. *Ecology* 85(8):2184–2199.
4. Samanta A, et al. (2010) Amazon forests did not green-up during the 2005 drought. *Geophys Res Lett* 37(5):L05401, 10.1029/2009GL042154.
5. Ciais Ph, et al. (2005) Europe-wide reduction in primary productivity caused by the heat and drought in 2003. *Nature* 437(7058):529–533.
6. Vicente-Serrano SM, Beguería S, López-Moreno JI (2011) Comment on "Characteristics and trends in various forms of the Palmer Drought Severity Index (PDSI) during 1900-2008" by A. Dai. *Journal of Geophysical Research-Atmosphere* 116(19):D19112, 10.1029/2011JD016410.
7. Breshears DD, et al. (2005) Regional vegetation die-off in response to global-change-type drought. *Proc Natl Acad Sci USA* 102(42):15144–15148.
8. Allen CD, et al. (2010) A global overview of drought and heat-induced tree mortality reveals emerging climate change risks for forests. *For Ecol Manage* 259(4):660–684.
9. Chaves MM, Maroco JP, Pereira JS (2003) Understanding plant responses to drought—From genes to the whole plant. *Funct Plant Biol* 30(3):239–264.
10. McDowell N, et al. (2008) Mechanisms of plant survival and mortality during drought: Why do some plants survive while others succumb to drought? *New Phytol* 178(4): 719–739.
11. Pasho E, Camarero JJ, de Luis M, Vicente-Serrano SM (2011) Impacts of drought at different time scales on forest growth across a wide climatic gradient in north-eastern Spain. *Agric For Meteorol* 151(12):1800–1811.
12. Ji L, Peters AJ (2003) Assessing vegetation response to drought in the northern Great Plains using vegetation and drought indices. *Remote Sens Environ* 87(1):85–98.
13. Adams HD, et al. (2009) Temperature sensitivity of drought-induced tree mortality portends increased regional die-off under global-change-type drought. *Proc Natl Acad Sci USA* 106(17):7063–7066.
14. McKee TBN, Doesken J, Kleist J (1993) The relationship of drought frequency and duration to time scales. *Eighth Conference on Applied Climatology* (American Meteorological Society, Anaheim, CA), pp 179–184.
15. Vicente-Serrano SM (2007) Evaluating the impact of drought using remote sensing in a Mediterranean, semi-arid region. *Nat Hazards* 40(1):173–208.
16. Huxman TE, et al. (2004) Convergence across biomes to a common rain-use efficiency. *Nature* 429(6992):651–654.
17. Vicente-Serrano SM, Beguería S, López-Moreno JI (2010) A multi-scalar drought index sensitive to global warming: The Standardized Precipitation Evapotranspiration Index – SPEI. *J Clim* 23(17):1696–1718.
18. Vicente-Serrano SM, et al. (2012) Performance of drought indices for ecological, agricultural and hydrological applications. *Earth Interact* 16(10):1–27.
19. Schuur EAG (2003) Productivity and global climate revisited: The sensitivity of tropical forest growth to precipitation. *Ecology* 84(5):1165–1170.
20. Phillips OL, et al. (2009) Drought sensitivity of the Amazon rainforest. *Science* 323 (5919):1344–1347.
21. Xu L, et al. (2011) Widespread decline in greenness of Amazonian vegetation due to the 2010 drought. *Geophys Res Lett* 38(7):L07402, 10.1029/2011GL046824.
22. Stephenson NL (1990) Climatic control of vegetation distribution: The role of the water balance. *Am Nat* 135(5):649–670.
23. Stegen JC, et al. (2011) Variation in above-ground forest biomass across broad climatic gradients. *Glob Ecol Biogeogr* 20(5):744–754.
24. Engelbrecht BMJ, et al. (2007) Drought sensitivity shapes species distribution patterns in tropical forests. *Nature* 447(7140):80–82.
25. Pockman WT, Sperry JS (2000) Vulnerability to xylem cavitation and the distribution of Sonoran Desert vegetation. *Am J Bot* 87(9):1287–1299.
26. Schwinning S, Sala OE (2004) Hierarchy of responses to resource pulses in arid and semi-arid ecosystems. *Oecologia* 141(2):211–220.
27. Lundholm B (1976) Adaptations in arid ecosystems. *Can Desert Encroachment Be Stopped? Ecological Bull. No. 24*, eds Rapp A, Le Houerou NH, Lundholm B (United Nations Environmental Programme, Stockholm, Sweden).
28. Barber VA, Juday GP, Finney BP (2000) Reduced growth of Alaskan white spruce in the twentieth century from temperature-induced drought stress. *Nature* 405(6787): 668–673.
29. Anderegg WRL, et al. (2012) The roles of hydraulic and carbon stress in a widespread climate-induced forest die-off. *Proc Natl Acad Sci USA* 109(1):233–237.
30. Bréda N, Huc R, Granier A, Dreyer E (2006) Temperate forest trees and stands under severe drought: A review of ecophysiological responses, adaptation processes and long-term consequences. *Ann For Sci* 63(16):625–644.
31. Phillips OL, et al. (2010) Drought-mortality relationships for tropical forests. *New Phytol* 187(3):631–646.
32. del Cacho M, Lloret F (2012) Resilience of Mediterranean shrubland to a severe drought episode: The role of seed bank and seedling emergence. *Plant Biol (Stuttg)* 14(3):458–466.
33. Lapenis A, Shvidenko A, Shepaschenko D, Nilsson S, Aiyyer A (2005) Acclimatation of Russian forests to recent changes in climate. *Glob Change Biol* 11(12):2090–2102.
34. Galiano L, Martínez-Vilalta J, Lloret F (2010) Drought-induced multifactor decline of Scots Pine in the Pyrenees and potential vegetation change by the expansion of co-occurring oak species. *Ecosystems (N Y)* 13(7):978–991.
35. Vicente-Serrano SM, Zouber A, Lasanta T, Pueyo Y (2012) Dryness is accelerating degradation of vulnerable shrublands in semiarid Mediterranean environments. *Ecol Monogr* 82(4):407–428.
36. Craine JM, et al. (2012) Global diversity of drought tolerance and grassland climate-change resilience. *Nature Climate Change*, 10.1038/nclimate1634.
37. Heumann BW, Seaquist JW, Eklundh L, Jönsson P (2007) AVHRR derived phenological change in the Sahel and Soudan, Africa, 1982-2005. *Remote Sens Environ* 108(4): 385–392.
38. Bonet A (2004) Secondary succession of semiarid Mediterranean old-fields in south-eastern Spain: Insights for conservation and restoration of degraded lands. *J Arid Environ* 56(2):213–233.
39. Lloret F, Siscart D, Dalmases C (2004) Canopy recovery after drought dieback in holm-oak Mediterranean forests of Catalonia (NE Spain). *Glob Change Biol* 10(12): 2092–2099.
40. Brando PM, et al. (2010) Seasonal and interannual variability of climate and vegetation indices across the Amazon. *Proc Natl Acad Sci USA* 107(33):14685–14690.
41. Solomon S, et al. (2007) *Climate Change 2007: The Physical Science Basis* (Cambridge Univ Press, Cambridge, UK).
42. Smith SD, et al. (2000) Elevated CO2 increases productivity and invasive species success in an arid ecosystem. *Nature* 408(6808):79–82.
43. Nemani RR, et al. (2003) Climate-driven increases in global terrestrial net primary production from 1982 to 1999. *Science* 300(5625):1560–1563.
44. Dai A (2012) Increasing drought under global warming in observations and models. *Nature Climate Change*, 10.1038/nclimate1633.
45. Beguería S, Vicente-Serrano SM, Angulo M (2010) A multi-scalar global drought data set: The SPEIbase: A new gridded product for the analysis of drought variability and impacts. *Bull Am Meteorol Soc* 91(10):1351–1354.
46. Tucker CJ, et al. (2005) An extended AVHRR 8-km NDVI data set compatible with MODIS and SPOT Vegetation NDVI Data. *Int J Remote Sens* 26(20):4485–5598.
47. Huete A, et al. (2002) Overview of the radiometric and biophysical performance of the MODIS vegetation indices. *Remote Sens Environ* 83(1-2):195–213.
48. Holdridge LR (1947) Determination of world plant formations from simple climatic data. *Science* 105(2727):367–368.
49. Peters AJ, et al. (2002) Drought monitoring with NDVI-based Standardized Vegetation Index. *Photogramm Eng Remote Sensing* 68(1):71–75.

SUPPLEMENTARY INFORMATION

The response of vegetation to drought time-scales across global land biomes

Sergio M. Vicente-Serrano[a], Célia Gouveia[b,c], Jesús Julio Camarero[d], Santiago Beguería[e], Ricardo Trigo[b,f], Juan I. López-Moreno[a], César Azorín-Molina[a], Edmond Pasho[a], Jorge Lorenzo-Lacruz[a], Jesús Revuelto[a], Enrique Morán-Tejeda[a] and Arturo Sanchez-Lorenzo[g]

[a]Instituto Pirenaico de Ecología, Consejo Superior de Investigaciones Científicas, Zaragoza, Spain 50059; [b]CGUL, IDL, Faculdade de Ciências, Universidade de Lisboa, Portugal; [c]Escola Superior de Tecnologia, Instituto Politécnico de Setúbal, Setúbal, Portugal; [d]ARAID-Instituto Pirenaico de Ecología; [e]Estación Experimental de Aula Dei, Consejo Superior de Investigaciones Científicas, Zaragoza, Spain; [f]Departamento de Engenharias, Universidade Lusófona, Lisboa, Portugal; [g]Institute for Atmospheric and Climate Science, ETH Zurich, Zurich, Switzerland

This document contains:

1. Supplemental material and methods

1.1. Drought index and dataset

Substantial efforts have been devoted for developing methods to quantify drought severity. The main efforts have been directed at developing drought indices that enable earlier identification of droughts, and quantification of their severity and spatial extent. Several drought indices were developed during the 20th century, based on a range of variables and parameters (S1-S4).

Most studies related to drought analysis have been conducted using either (i) the Palmer Drought Severity Index (PDSI) (S5), based on a soil water balance equation, or (ii) the Standardized Precipitation Index (SPI) (S6), based on a precipitation probabilistic approach. The PDSI has numerous deficiencies (6) but the main problem for the identification of drought impacts is that the PDSI has a fixed temporal scale (S7) whereas it is commonly accepted that drought is a multi-scalar phenomenon since the period from the water shortages to impacts in a given system differs noticeably. Drought is a phenomenon that may occur simultaneously across multiple temporal scales (e.g., a short period of particular dryness embedded within a long-term drought). Therefore, "multiple" refers to numerous, temporal periods that may or may not overlap. Thus, drought indices must be associated with a specific time scale to be useful for monitoring drought impacts of different nature. This explains the wide acceptance of the SPI, which is comparable in time and space (S7,S8), and can be calculated at different time scales. The SPI has been accepted by the World Meteorological Organization as the reference drought index (S9). Thus, a number of studies have demonstrated variation in the response at different time scales of the SPI to different hydrological (S10-S13); agricultural (S14,S15) and ecological variables (11,12,15).

The main criticism for the SPI is that its calculation is based only on precipitation data. The index does not consider other variables that can influence droughts, mainly the evapotranspirative demand by the atmosphere. Abramopoulos et al. (S16) used a general circulation model experiment to show that evaporation and transpiration can consume up to 80% of rainfall. The role of warming-induced drought stress is evident in recent studies that have analysed drought impacts on net primary production and tree mortality (S17-S21). The strong role of temperatures on the drought severity was evident in the devasting 2003 central European heat wave, in which extreme high temperatures dramatically increased evapotranspiration and exacerbated summer drought stress (S22), drastically reducing Aboveground Net Primary Production (ANPP) (5). Similar patterns were observed in the summer 2010 with a strong heat wave that increased drought stress in forests and produced large forest fires in eastern Europe and Russia (S23). Thus, empirical studies have demonstrated that higher temperatures increase drought stress and enhance forest mortality under precipitation shortages (13). Warming processes are also probably the triggering factor of the decline in world agricultural productions observed in the last years (S24). Thus, to illustrate how warming processes are reinforcing drought stress and related ecological impacts worldwide, Breshears et al. (7) enunciated the term global-change-type drought to refer to drought under global warming conditions.

Therefore, the use of drought indices which include temperature data in their formulation (such as the PDSI) is preferable to identify drought impacts on vegetation activity and growth. However, the PDSI lacks the multi-scalar character, essential to assess the different times of response of global vegetation communities to drought. For this reason, in this study we used a recently formulated drought index: the Standardized Precipitation Evapotranspiration Index (SPEI) based on precipitation (P) and Potential Evapotranspiration (PET) (17). The SPEI combines the sensitivity of PDSI to changes in evaporation demand (caused by temperature fluctuations and trends) with the multi-temporal nature of the SPI.

The SPEI is calculated by means of a climatic water balance i.e. the difference between precipitation and PET:

$$D = P - PET,$$

The calculated D values are aggregated at various time scales:

$$D_n^k = \sum_{i=0}^{k-1} \left(P_{n-i} - PET_{n-i} \right), \; n \geq k$$

where k (months) is the timescale of the aggregation and n is the calculation number. The D values are undefined for $k > n$. Timescales from 1- to 24-months were used in this study. For example, to obtain the 6-month SPEI, first a time series is constructed by the sum of D values from five months before to the current month. Given the strong seasonal differences in the magnitude of P and PET and the climate regimes of each site, to obtain SPEI series comparable in space and time, it is necessary to transform the D series using equal probability to a normal distribution with a mean of zero and standard deviation of one so the values of the SPEI are really in standard deviations and lacks of seasonal effects. A log-logistic probability distribution function is fitted to the data series of D, as it adapts very well to all time scales. The complete calculation procedure for the SPEI can be found in Vicente-Serrano et al. (17).

At the shortest time scales (e.g. three months) there is a continuous alternation of short dry (negative SPEI values) and humid (positive SPEI values) periods (Figure S9). Highly plastic vegetation acclimated to this high frequency variability in moisture conditions in drought-prone areas and vegetation not so well adapted to withstand drought stress are expected to respond to these short-time droughts differently. At longer time scales (e.g., 12-24 months) droughts are less frequent and last more than at shorter scales. Vegetation well adapted to

withstand drought is also expected to respond to these time scales since it could be relatively insensitive to droughts acting at shorter time scales whereas persistent and sustained droughts acting at longer time scales might negatively affect plant communities from drought-prone areas.

The SPEI data has been obtained from the SPEIbase (45,S25), which is based on the CRU TS3.0 monthly precipitation and mean temperature dataset, compiled and processed by the Climate Research Unit of the University of East Anglia (http://badc.nerc.ac.uk/view/badc.nerc.ac.uk_ATOM_dataent_1256223773328276).

1.2. Assessment of the global aridity conditions

There are different indices proposed to assess the aridity of a region (S26-S28). All of these indices are based on values of precipitation and temperature or Potential Evapotranspiration (PET). The Environmental Programme of the United Nations (S29), proposed a drought index based on the quotient between precipitation and potential evapotranspiration. The quotient diminishes the role of the PET in relation to the precipitation on the aridity conditions. Then, to have an assessment of the global aridity we opted to calculate a simple climatic water balance based on the difference between the average annual precipitation and the average PET, which provides a quantification of the available deficit or surplus of water in each site. The PET was calculated according to the Thorthwaite equation (S27) since it only requires data of temperature to be calculated. Although the reference method accepted to estimate the PET by the Food and Agricultural Organization (FAO) is based on the Penmann-Monteith equation, it requires of several meteorological variables to be calculated (wind speed, solar radiation, relative humidity and temperature) which are not available at the global scale of the present study. Therefore, we opted for the use of the Thornthwaite equation (albeit slightly less accurate than other more complex approaches), given the low requirements of data and the general good results that it provides since it allows identifying the existing evapotranspiration differences at a global scale (Figure S10).

1.3. Quantifying vegetation activity from remote sensing images

At present the unique available empirical information at a global scale and the sufficient spatial resolution to identify differences between vegetation communities, mainly in areas of high spatial diversity in vegetation activity, is obtained from remote sensing images collected from earth observation satellites.

When the sun electromagnetic radiation reaches the plant leaves, a part of the energy is reflected and the rest is absorbed or transmitted. Nevertheless, the response of the active vegetation to the energy received at different longwaves is quite different. In the visible part of the electromagnetic spectrum there is a great energetic absorption due the vegetation pigments and to the energetic consumption by photosynthesis. On the contrary, in the region of the near infrared, most of the radiation is reflected as a consequence of the internal structure of the leaves (S30, S31).

It is possible to summarise the information received in the red and infrared regions of the spectrum by radiometers and to obtain a measure of the vegetation activity. This is commonly done by means of vegetation indices, which are combinations of spectral bands with the objective of emphasizing the photosynthetic active components (S32). Several vegetation indices have been developed (S33, S34). Nevertheless, at present the most extended and widely used index is the Normalized Difference Vegetation Index (NDVI) which is formulated as (S35):

$$NDVI = \frac{\rho_{NIR} - \rho_{red}}{\rho_{NIR} + \rho_{red}}$$

where ρ_{NIR} and ρ_{red} are the reflectance values of the near infrared and red bands, respectively. The NDVI has been shown to be highly correlated with vegetation parameters such as green leaf biomass and green leaf area (S36-S39) and it is an excellent proxy of the photosynthetic activity (S40,S41). The NDVI has also some limitations to analyse the dynamics of the vegetation activity because: i) the relationship between vegetation parameters (leaf area, ANPP, plant cover, etc.) and the NDVI are sometimes non-linear since the NDVI saturates before the maximum biomass is reached (S42,S43), ii) when canopy cover is sparse, there are substantial spectral background contributions (e.g. soil) to the overall remote sensing signal and iii) it is influenced by the amount of clear sky days and the level of atmospheric aerosols. Nevertheless, numerous authors have demonstrated the strong relationship existing between the NDVI and the leaf area index (S44) and the total vegetation biomass (S45-S48). Thus, recent studies have also shown that variations of the near infrared reflectance as a consequence of changes in the leaf water potential, which are associated with drought, are also observed in dense forests (S49). These findings indicate that even in these dense areas the NDVI can also record spectral variations associated with changes in vegetation activity related to drought. In addition, in dense forests of the Amazonian Basin, Brando et al. (40) have shown a significant association between the production of new leaves by trees and the values of the satellite-derived vegetation indices, which provides evidence on the sensibility of the vegetation spectral indices to changes in the tree activity and biomass of very dense forests. In any case, to provide more robustness to our results, we have also used improved vegetation indices obtained from recent satellite platforms that reduce the commented problems attributed to the NDVI (see below).

1.4. Vegetation activity datasets

Currently, there are several satellites recording land spectral information that allows quantifying the NDVI or

other vegetation indices. Among them, the unique satellites that record with a high temporal resolution global data are the NOAA, the SPOT-VEGETATION and the TERRA/AQUA satellites. The main problem of the satellite imagery recorded by these satellites is the short range of the available time series. The SPOT-VEGETATION data is available from the launching of the SPOT-VGT1 in 1998 and MODIS images are available from 2001. These periods are too short to obtain reliable conclusions about the drought impacts on vegetation activity. The longest time-series of satellite imagery at a global scale with the spectral bands that may obtain the NDVI are from the NOAA satellites since the first operative satellite with robust calibration was launched in 1981 (NOAA-7). Different NOAA satellites have been launched since 1981, but all of them have used the same sensor: the Advanced Very High Resolution Radiometer (AVHRR), which records information in the spectral band of the red and near infrared and allows calculating the NDVI (S50). In addition, the AVHRR data are recorded daily in any part of the world, which ensures availability of images with a high temporal frequency, independently of the cloud coverage.

Nevertheless, the precision of the NDVI time series obtained from NOAA-AVHRR images have problems related to the temporal homogeneity and stability of the NOAA satellites (S51) since the satellite changes and the orbit degradations may affect noticeably the derived NDVI products (S52).

Given the great applicability of the available NOAA-AVHRR images, different research and earth observation organisms have devoted a great effort to create long-term homogeneous NDVI datasets at a global scale and at the spatial resolution of the AVHRR Global Area Coverage, i.e. a grid size of 8 x 8 km. A review of the available datasets has been recently published (S53). Among the existing datasets, we have selected the NOAA Global Inventory Modeling and Mapping Studies (GIMMS) Normalized Difference Vegetation Index (NDVI) (46) since it covers a longer period than the other existing datasets (1981-2006). The NOAA GIMMS NDVI data were generated from the original 1.1 km^2 NOAA AVHRR data as bi-weekly maximum value composites aggregated to an 8 x 8 km pixel resolution. The quality and consistency of the GIMMS data were assured by the correction for i) sensor degradation, ii) sensor inter-calibration differences, iii) solar zenith and viewing angles, iv) volcanic aerosols, v) atmospheric water vapour and vi) cloud cover. By comparing NOAA GIMMS and Landsat images, Beck et al. (S53) have shown that the GIMMS is the most accurate AVHRR-NDVI dataset for assessing vegetation variability and trends.

The new MODIS sensor on board of the satellites AQUA and TERRA shows improved capabilities regarding previous satellite platforms (S54). The higher number of spectral bands of the MODIS sensor in comparison to the AVHRR allows calculating additional vegetation indices. Among them, the Enhanced Vegetation Index (EVI) (S55, S56) was developed to optimize the vegetation signal with improved sensitivity in high biomass regions and enhanced vegetation monitoring and a reduction in atmosphere influences. The EVI has been widely used in the last years since it is more responsive to canopy structural variations, including leaf area index (LAI), canopy type, plant physiognomy, and canopy architecture than NDVI (S56). For this reason, although the MODIS data encompass a much shorter period of data as compared with the GIMMS-NDVI dataset since the former has only 9 years of common data with the SPEIbase (2001-2009), we have also included the EVI and NDVI datasets from the MODIS Collection 5 (C5) in the analyses (S57).

1.5. Tree-ring growth data

We compiled 1846 tree-ring width chronologies encompassing the period 1945-2009 archived by the National Climate Data Center (NCDC) in the the International Tree-Ring Data Bank (ITRDB) (S58). These annually resolved archives are kindly provided by dendrochronologists and are available online at: http://www.ncdc.noaa.gov/paleo/treering.html. Each chronology represents the average radial growth series of several trees (typically more than ten) of the same species growing in the same site. The wood samples are taken following standard protocols which include sampling at least ten trees within a local population, taking usually two radial cores per tree at 1.3 m. The selected 1846 sites corresponded to those chronologies listed in the ITRDB in November 2011 with at least ten trees sampled after 1940, which we regarded as an acceptable criterion for robust replication within each site. Most sites with tree-ring width data available at the ITRDB were located in North America and Europe (Figure S11).

Wood samples are air-dried and polished using sand-papers of progressively finer grain or transversally sectioned until tree-rings are clearly visible under a binocular. Then, they are visually cross-dated using characteristic rings (S59). The ring widths of cross-dated samples are measured using semi-automatic devices usually with a resolution of 0.01 mm. Then, the visual cross-dating of measured samples is checked with the COFECHA program which calculates correlations between the individual series measured for each radius and the mean average series considering fixed time intervals (S60). All conversions among the different formats used by the dendrochronological community were done using the TriCycle program to obtain decadal files (S61).

Raw ring-width measurements were standardized to remove long term biological growth trends associated with tree ageing and increasing trunk diameter, but to preserve interannual and interdecadal variability, often associated with climate variability including changes in SPEI (11). Standardizations were carried out by the original scientists who contributed the chronologies to the ITRDB (see a similar analysis in S62). Usually, individual series of tree-ring widths were fitted with negative exponential curves or linear functions and

residuals were obtained by dividing the observed by the fitted values. The resulting width residuals were subjected to autorregressive modelling and then averaged for each year using a biweight robust mean to obtain a mean residual chronology of prewhitened growth indices for each site. The detrending procedure was performed using the program ARSTAN (S63). In the case of long chronologies (length > 300 years) corresponding to forests with old trees, trends in ring-width indices for the late 20th century were further removed by fitting linear regressions and keeping the resulting residuals.

1.6. Methods

The procedure followed to calculate the correlations between the SPEI series and the series of the three vegetation parameters is illustrated in Figure S12. It corresponds to the GIMMS-NDVI in a warm temperate thorn scrub in South Africa (25.9ºE, 25.9ºS). It shows the evolution of the March standardized NDVI and the March series of SPEI at the time scales of 1, 3 and 12 months and it is clear that there is a close agreement between the NDVI and the 3-month SPEI. Thus, considering all the SPEI time scales, from 1 to 24 months, maximum correlation is recorded at the 3-month time scale, which means that the magnitude of the NDVI in March is mostly determined by the cumulative water balance occurring from January to March. Therefore, both, the maximum correlation recorded (0.68) and the 3-month time-scale are retained for further analysis. The same approach is applied to the tree-ring growth and ANPP, but given that the series are annual, they are correlated with the 1- to 24-month SPEI series of each month of the year, identifying the month of the year and the SPEI time scale at which maximum correlation is reach, and the magnitude of the maximum correlation.

We obtained monthly maps of relationships between GIMMS and MODIS vegetation indices and different time scales of the SPEI (Figure S13). The maps A to D represent the correlations found between the time series of May GIMMS-NDVI and that of May SPEI at the time scales of A) 3, B) 6, C) 12 and D) 18 months. The figures show similarities and differences in the spatial patterns and magnitude of correlations. The plot E) shows the maximum correlation for May between the SPEI and the GIMMS-NDVI, which is a composite map created from the correlations indicated in the maps A) to D) and also including other SPEI time scales (from 1 to 24 months). The plot E) shows the maximum correlation found between NDVI and SPEI at time scales ranging from 1 to 24 months. The plot F) represents the SPEI time scale at which the maximum correlations are found. The seasonal and annual maps were created by the maximum of the corresponding monthly correlation maps.

The influence of droughts on tree growth and ANPP was also assessed by means of the Pearson coefficient computed between the annual ANPP and tree-ring width series and the 1- to 24-month monthly SPEI series of the 0.5º grid that included the corresponding forest and ANPP sites. Therefore, for each tree-ring width series we also obtained 288 correlations. Maximum correlations and corresponding time scales were mapped and retained for further analyses. Since both low- to mid-frequency variability and the first-order autocorrelation were removed in the residual tree-ring series of prewhitened width indices to avoid the decreasing trend of tree-ring width as trees enlarge and age, the 1- to 24-month SPEI series were also detrended for the period of available tree-ring data between 1945 and 2006 before calculating correlations.

2. Supplemental Seasonal Analysis

Analyses on the SPEI time scales at which maximum correlations between the SPEI and the GIMMS-NDVI were observed are also provided seasonally (Figure S14) to identify the existing seasonal differences as a consequence of the vegetation phenology in the global vegetation. The relationship between the annual water balance across eco-regions versus the SPEI/GIMMS-NDVI maximum correlations (Figure S15) and the corresponding time scales at which these maximum correlations are found (Figure S16) are also shown. These figures clearly show small differences among seasons and a similar pattern to that shown at an annual scale.

3. Supplemental analysis of MODIS images

To strength the robustness of the obtained results with the GIMMS-NDVI dataset, analysis have been performed using EVI and NDVI data from the MODIS images between 2001 and 2009. The results show similar results to those indicated with the GIMMS-NDVI, both for the annual and seasonal analyses. The spatial distribution of the maximum annual correlations between SPEI and MODIS-EVI and –NDVI are shown in Figure S17. The seasonal maximum correlations are shown for the EVI and the NDVI in Figures S18 and S19, respectively. Areas with statistically significant correlations are shown in Figures S20 and S21 for EVI and NDVI datasets, respectively. The relationship between the SPEI/EVI and NDVI maximum correlations and the annual water balance across eco-regions is shown in Figure S22. The SPEI time scales at which maximum correlations between the SPEI and the MODIS EVI and NDVI are found are shown annually (Figure S23) and seasonally (Figures S24 and S25).

4. Supplemental Figures and Tables

Site	latitude	longitude	years of data	Type of vegetation	Source
Hopland field station	38.96	-123.1	16	Pasture	(S64)
Carey Kipuka	43.33	-113.53	10	Pasture	(S65)
Little Crater	42.87	-113.13	10	Pasture	(S65)
Hansel Valley	41.68	-112.58	10	Pasture	(S65)
Rattelsnake pass	41.86	-112.5	10	Pasture	(S65)
Morgan Pasture	43.45	-112.47	10	Pasture	(S65)
Kettle Butte	43.54	-112.43	10	Pasture	(S65)
Benmore	40.03	-112.4	11	Pasture	(S66)
Snake river plain	44.3	-112.3	13	Grasses and shrubs	(S67)
Manyberries	49.4	-110.68	50	Pasture	(S68)
Santa Rita	31.85	-110.57	10	Pasture	(S69)
Doña Ana	32.53	-106.86	32	Pasture	(S70)
Jornada	32.6	-106.7	19	Black grama grassland	(2)
Sevilleta	34.3	-106.6	10	Mixed desert grassland	(2)
Niwot Ridge	40.1	-105.6	15	Moist alpine meadow	(2)
Cheyenne	41.18	-104.88	17	Grassland	(S71)
Central Plains Experimental range	40.83	-104.7	50	Grassland steppe	(S72)
Sidney (Montana)	47.7	-104.15	12	Pasture	(S73)
Great Plains Field Station	46.81	-100.88	16	Pasture	(S74)
Missouri	46.76	-99.46	21	Pasture	(S75)
Hays	38.86	-99.31	24	Pasture	(S76)
Montecillo	19.46	-98.91	10	Saline Grassland	(S77)
Flint Hills	39.18	-96.58	42	Pasture	(S78)
East Bay Ballou	29.6	-94.41	13	Grasses	(S79)
Cedar Creek	45.4	-93.2	23	Oak savanna grassland	(2)
Kellogs	42.4	-85.4	10	Successional field	(2)
Barro Colorado	9.15	-79.85	11	Tropical forest	(S77)
Debordieu	33.33	-79.25	10	Wet forest	(S80)
Harvard Forest	42.48	-72.18	18	Mixed deciduous Forest	(2)
Hubbord Brook	43.9	-71.71	10	Mixed deciduous Forest	(2)
Patagonia Argentina	-45.68	-70.26	10	Pasture	(S81)
Sydenham	-29.1	27.25	19	Pasture	(S82)
Towoomba	-24.9	28.35	19	Fine-leaved savanna	(S77)
Migda	31.36	34.42	10	Pasture	(S83)
Yaakov	33.01	35.25	13	Pasture	(S84)
Kursk	51.67	36.5	29	Meadow steppe	(S77)
Dzhanybek	49.33	46.78	33	Semi-desert steppe	(S77)
Badkhyz	35.68	62	31	Desert steppe	(S77)
Xilin	43.63	116.7	24	Steppe	(S85)
San Joaquín	37.08	119.76	13	Pasture	(S86)
Tumugi	46.1	123	10	meadow steppe	(S77)
Paracou*	5	-52.08	11	Tropical forest	(S87)
Boukoko*	3.25	18	13	Tropical forest	(S87)
Sungei Menyala Forest Reserve*	2.46	101.91	13	Tropical forest	(S88)

Table S1. Series of Aboveground Net Primary Production (ANPP) used in this study. The location, years of data, type of vegetation and data sources are also included. Raw data was obtained from published tabular data or by digitizing figures. Positive and negative values for latitude and longitude correspond to N or S and E or W hemispheres, respectively. Given the difficulty of estimating ANPP in forest sites (S89), forest areas are underrepresented, mainly in tropical and equatorial areas. To limit this problem and given the close relationship found between annual stem wood production and ANPP (S90,S91), we have also included three time series of growth increments obtained in tropical forests. Series marked by * correspond to series of annual stem growth increments based on repeated measures of diameter at 1.3 m. Annual ANPP data published in the different studies is commonly obtained in the periods of peak biomass. In the case in which monthly data is published, we have selected the monthly series corresponding to the peak of vegetation biomass.

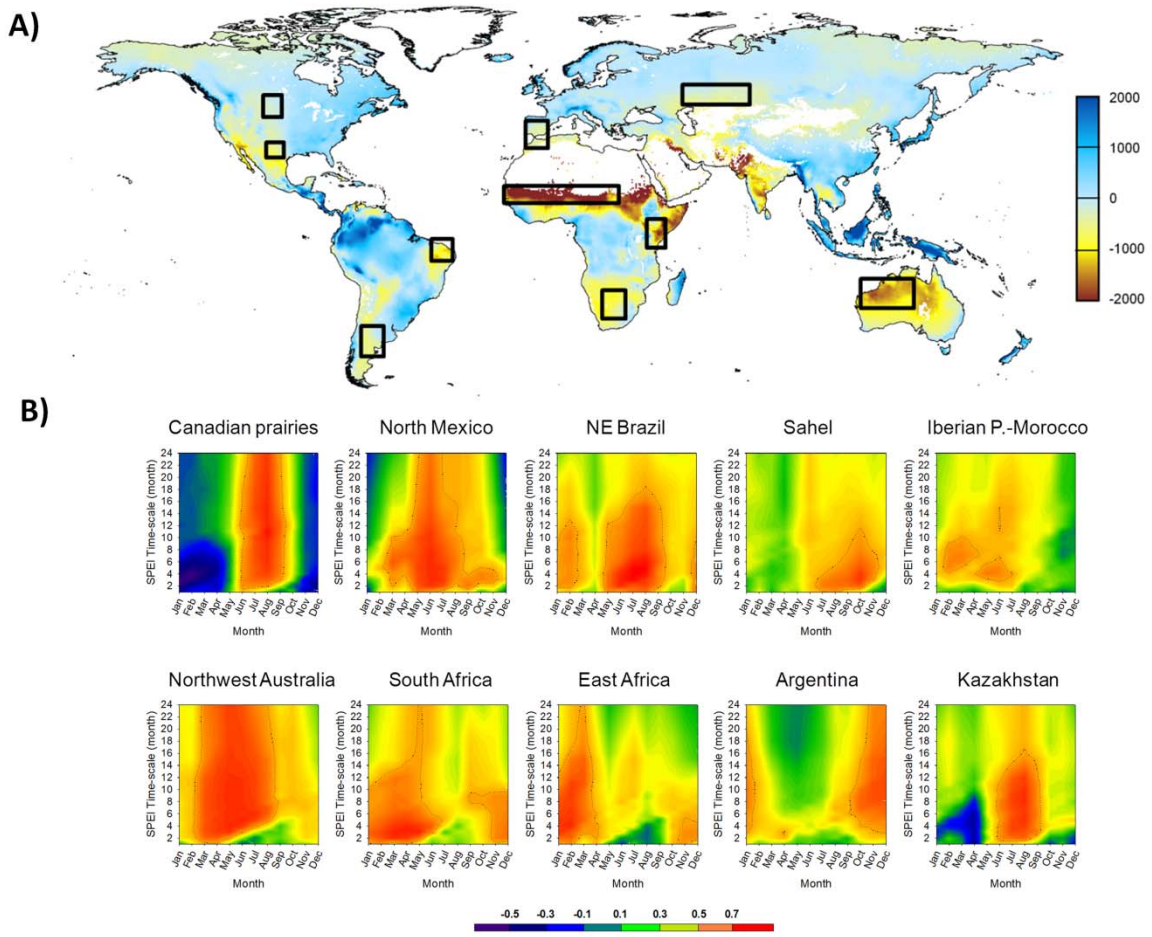

Figure S1. A) Average annual water balance (difference between annual precipitation and potential evapotranspiration in mm) for the period 1976-2006. Deserts are masked in white. **B)** Correlations (Pearson coefficient) between the SPEI at time scales from 1 to and 24 months and the GIMMS-NDVI in different regions of the world (see the map in A) for the period 1981-2006. Dotted lines frame statistically significant correlations ($\alpha < 0.05$). In the Canadian prairies drought determines, to a large extent, vegetation activity during the boreal summer, and the vegetation response seems to be insensitive to the drought time scale. However, in other areas (e.g. Argentina) the influence of drought is greatest at long time scales (> 8 months), while in the Sahel its effect mostly occurs at short ones (< 6 months). In some areas the vegetation response to drought can be more complex, even bimodal (e.g. NE Brazil and the Iberian Peninsula), as it can act at long and short time scales in seasonally specific responses.

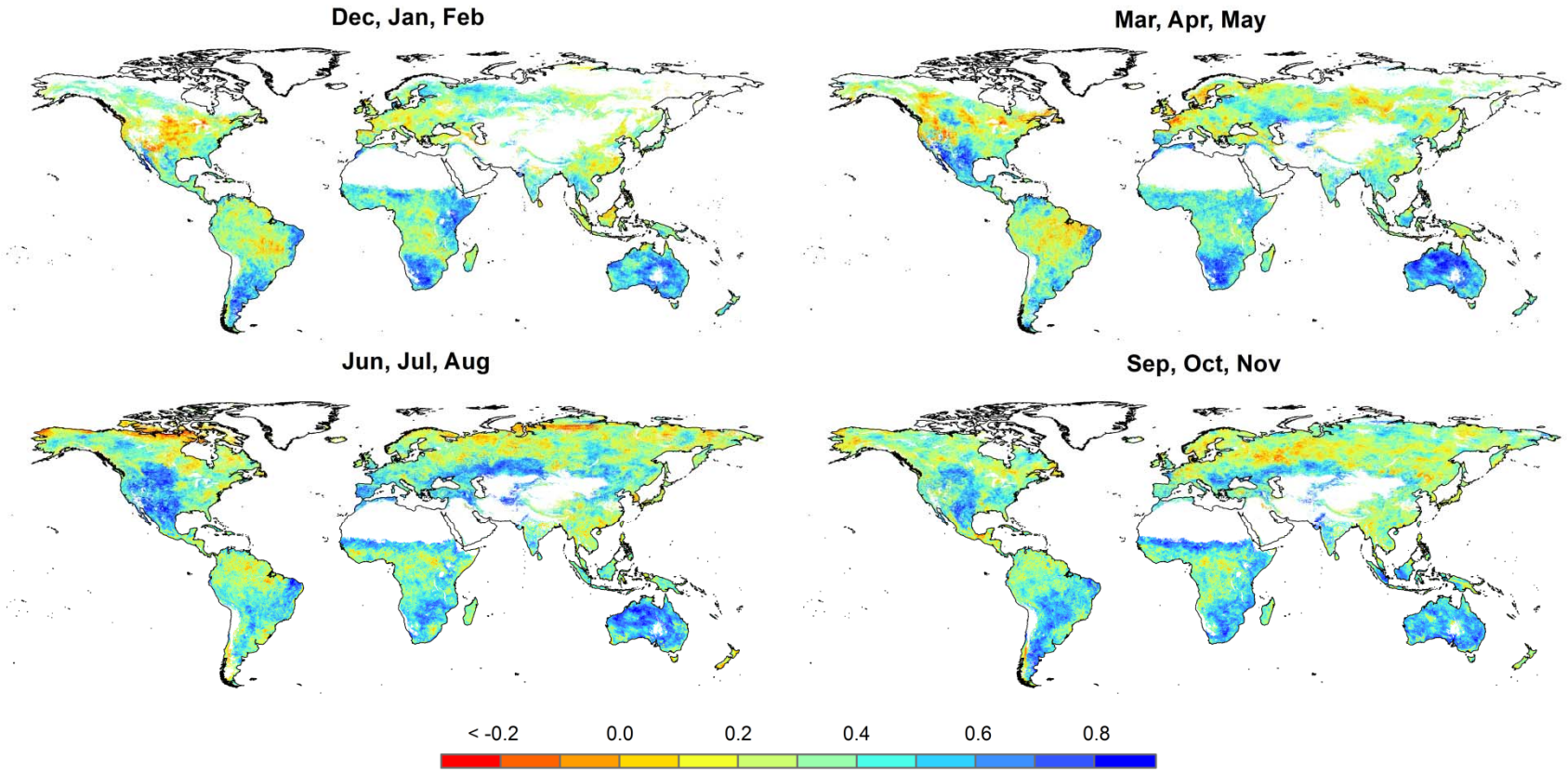

Figure S2. Spatial distribution of the seasonal correlations (Pearson coefficient) between SPEI and GIMMS-NDVI for the period 1981-2006. The values represent the maximum correlation (*r*) recorded for each pixel, independently of the month and the SPEI time scale. Desert and ice areas are masked and not included in the analysis.

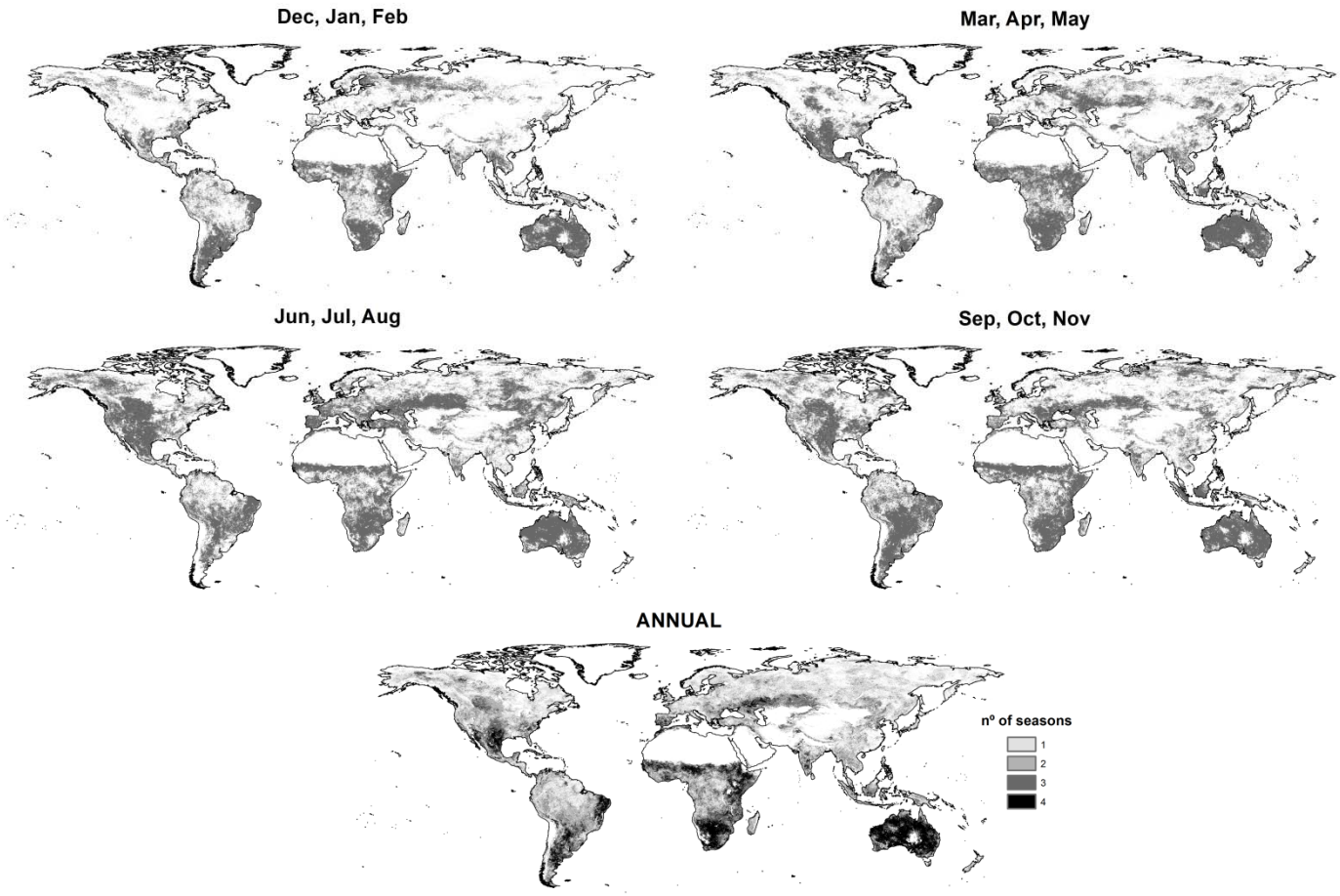

Figure S3. Areas with statistically significant Pearson correlation coefficients ($\alpha < 0.05$) between the SPEI and the GIMMS-NDVI calculated at seasonal and annual resolutions. The legend of the lowermost annual map indicates the number of seasons in which significant correlations were obtained.

Season	Surface (x 10^6 km^2)	% Total world	% vegetated areas
Dec.,Jan.,Feb.	97.53	23.60	43.92
Mar.,Apr.,May	113.28	28.38	45.47
Jun.,Jul.,Aug.	138.84	36.70	47.98
Sep.,Oct.,Nov.	133.55	35.16	47.80
Annual	218.40	57.50	72.00

Table S2. Surface of the world with significant Pearson correlation coefficients ($\alpha < 0.05$, $r > 0.38$) between the SPEI and the GIMMS-NDVI (1981-2006). The vegetated areas were obtained from the GlobCover dataset.

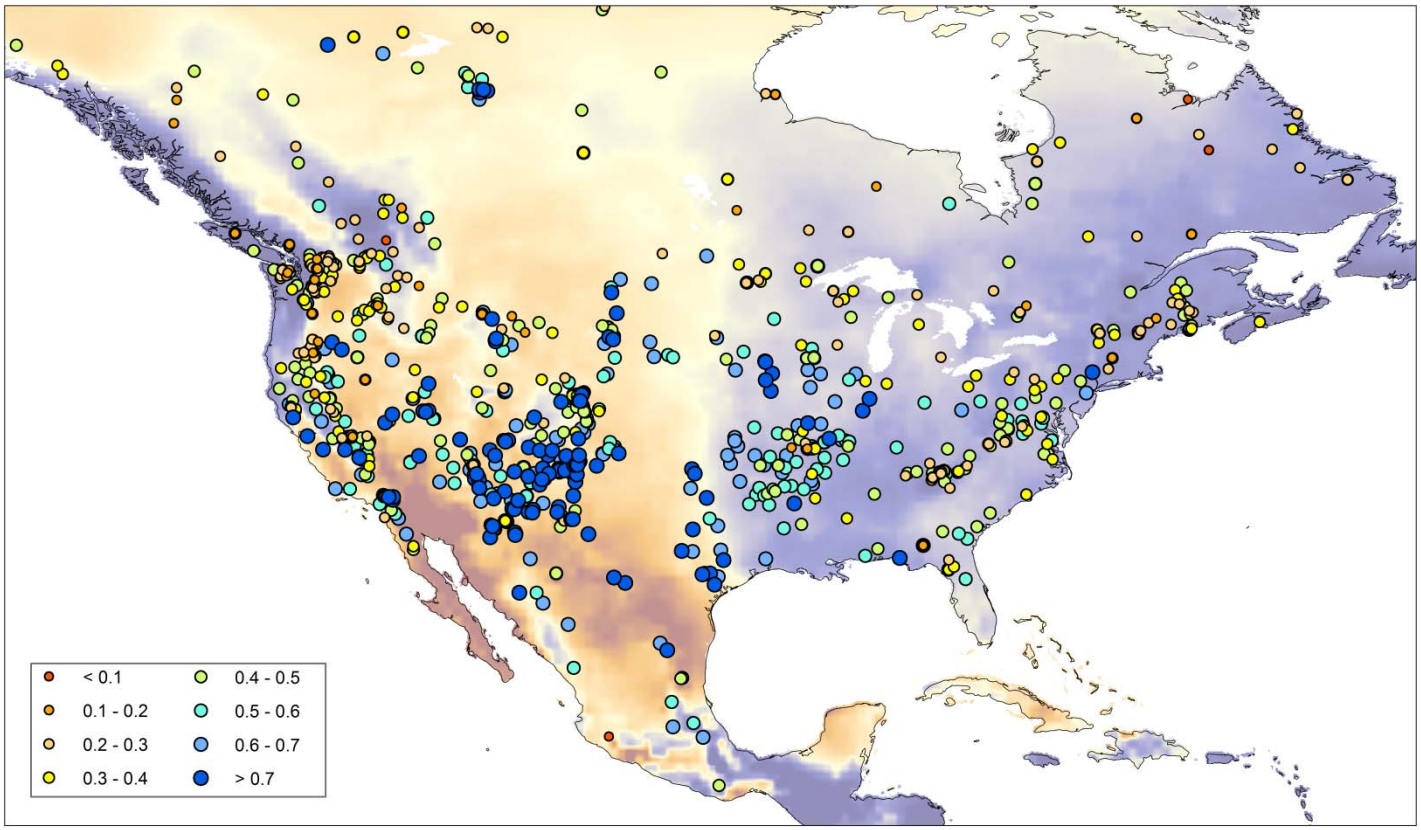

Figure S4. Spatial distribution of the correlations (Pearson coefficients, *r*) between SPEI and tree-ring width series for the period 1945-2009 in North America. The values represent the maximum correlation recorded for each pixel, independently of the month of the year and the SPEI time scale. The background colours represent the distribution of the water balance indicated in Figure S1.A.

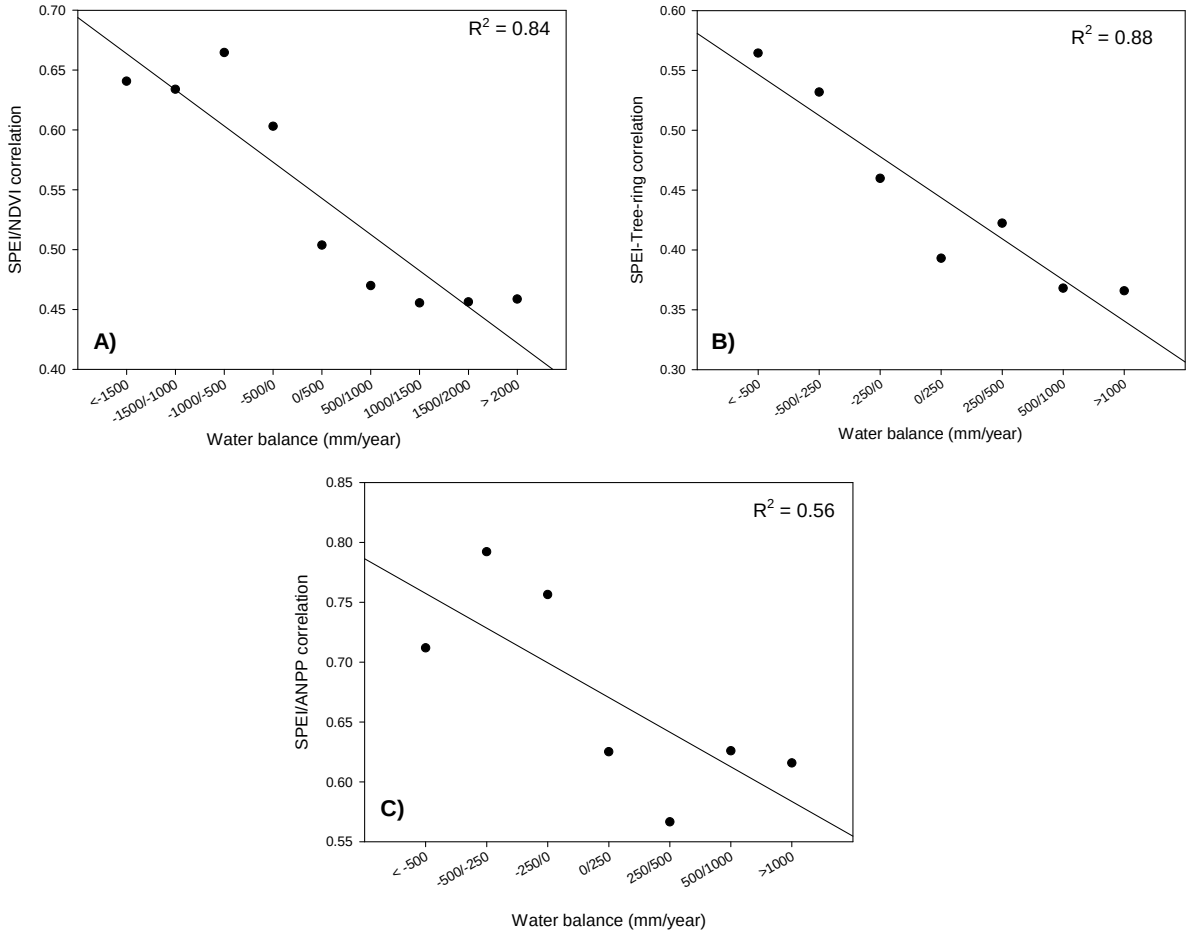

Figure S5. (A) Average values of the GIMMS-NDVI/SPEI maximum correlations summarized for different ranges of the annual water balance (precipitation minus PET), **(B)** Average values of the tree-ring width/SPEI maximum correlations summarized for different ranges of the annual water balance. **(C)** Average values of the ANPP/SPEI maximum correlations summarized for different ranges of the annual water balance. Results of the linear fitting by means of the coefficient of determination are also shown.

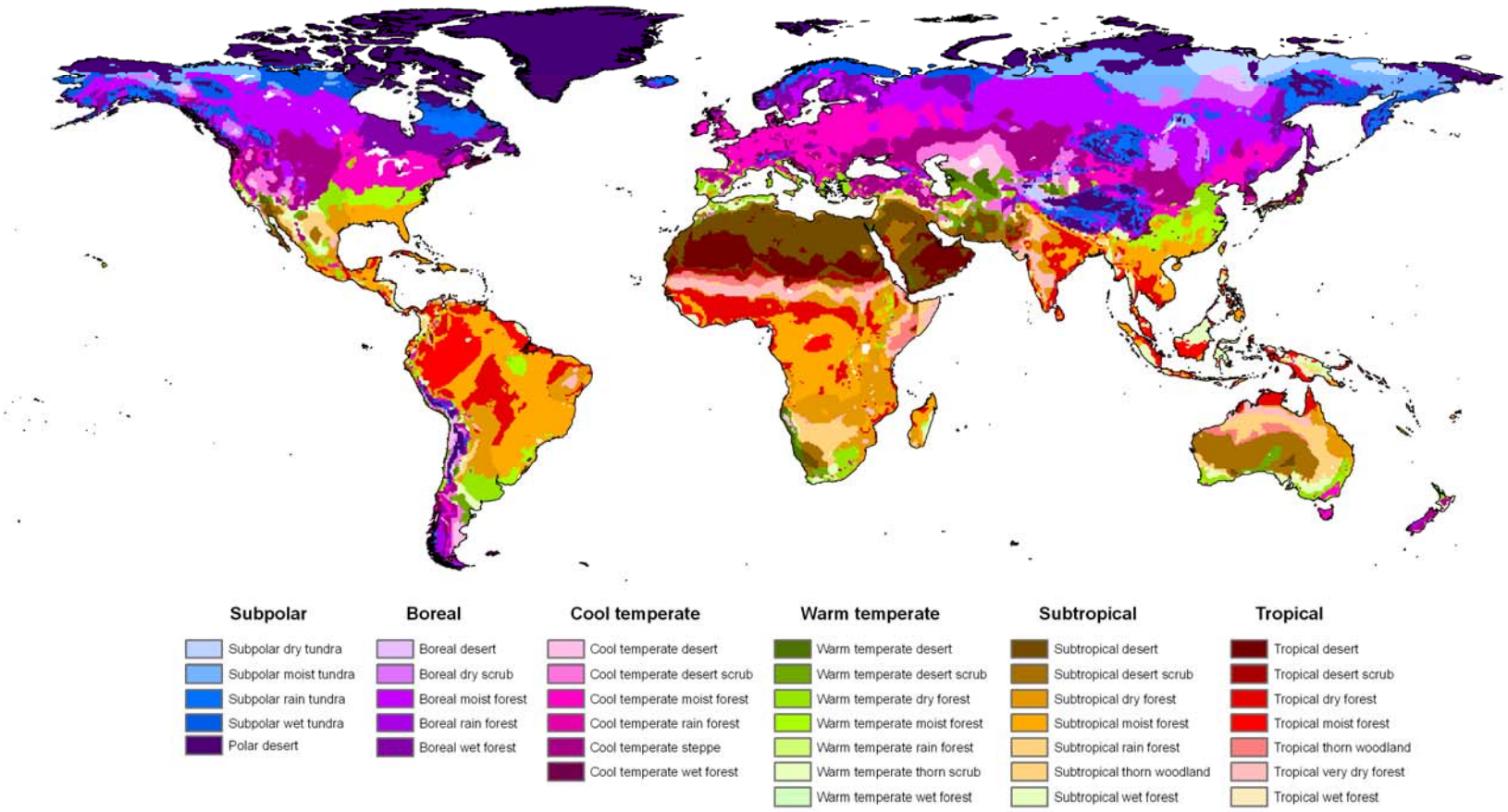

Figure S6. Map of the Holdridge classification system of eco-regions and biomes (48).

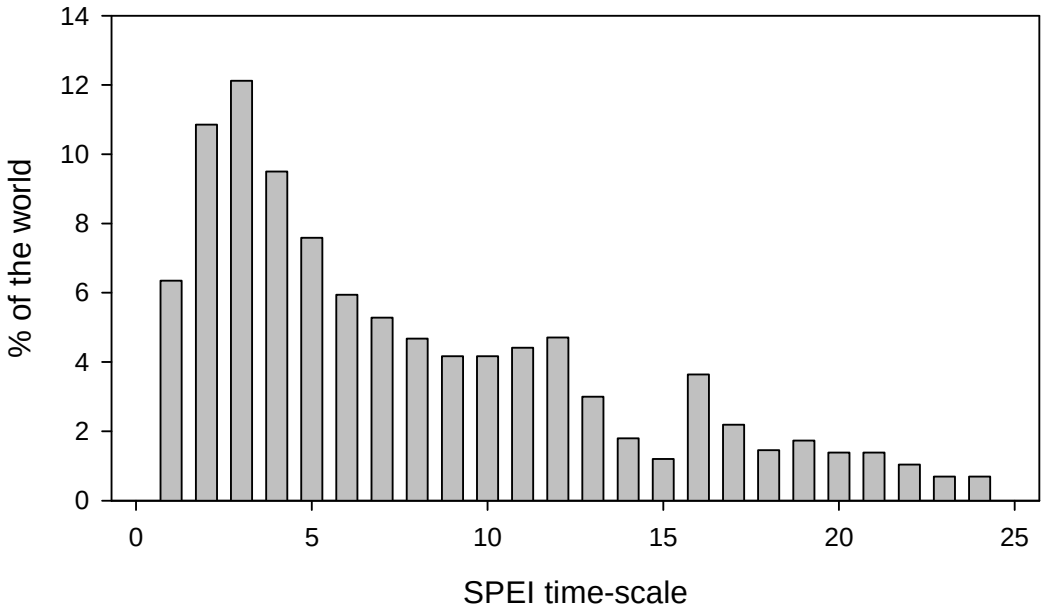

Figure S7. Percentage of the world terrestrial area covered by vegetation in which maximum GIMMS-NDVI/SPEI correlations are found at different SPEI time scales (in months).

A)

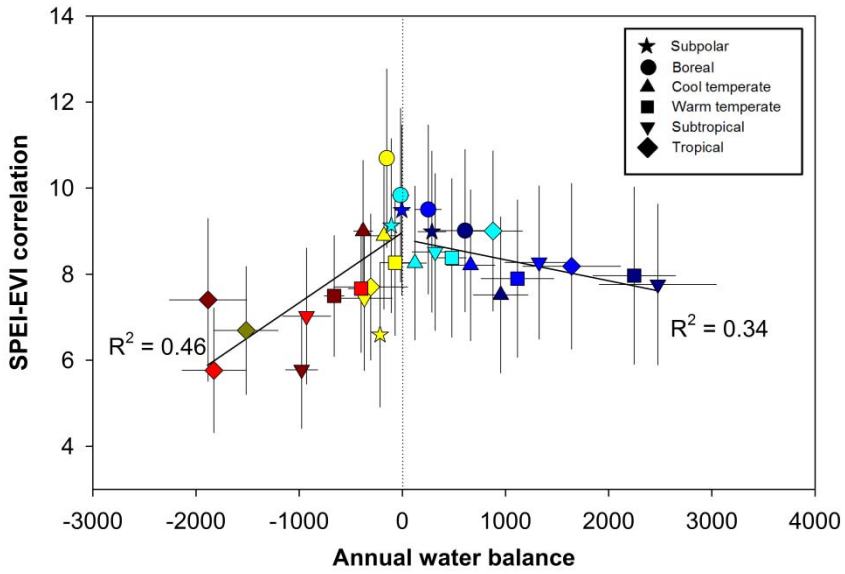

B)

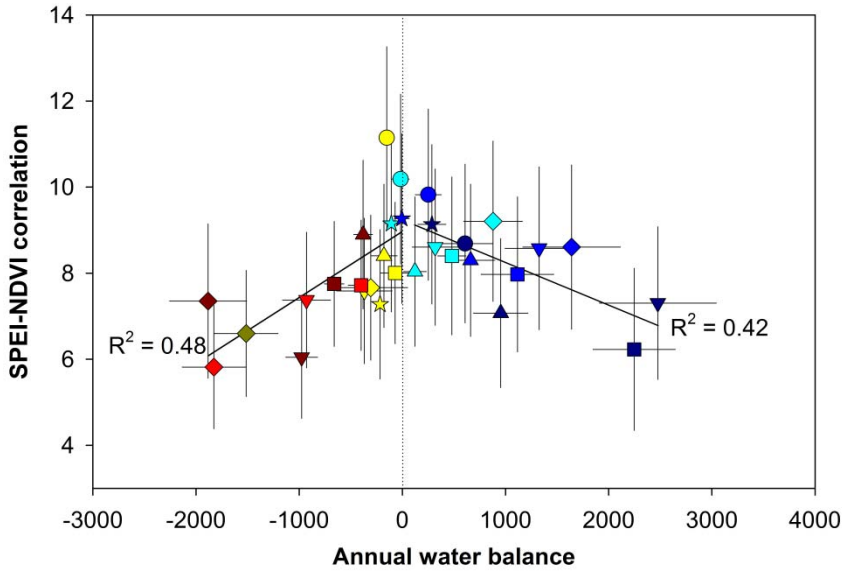

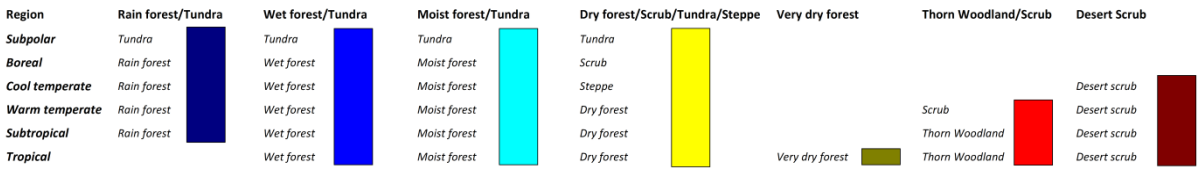

Figure S8. Relationship between the average SPEI time scales at which the maximum SPEI/MODIS **A)** –EVI and **B)** -NDVI correlation is found and the average annual water balance across eco-regions. The biomes are grouped according to the six existing eco-regions: Subpolar, Boreal, Cool temperate, Warm temperate, Subtropical and Tropical. Colors represent the different biomes of each one of the six eco-regions in the A and B plots and the symbols represent the different eco-regions.Results of the linear fitting by means of the coefficient of determination are also shown. Error bars represent ± ½ standard deviations.

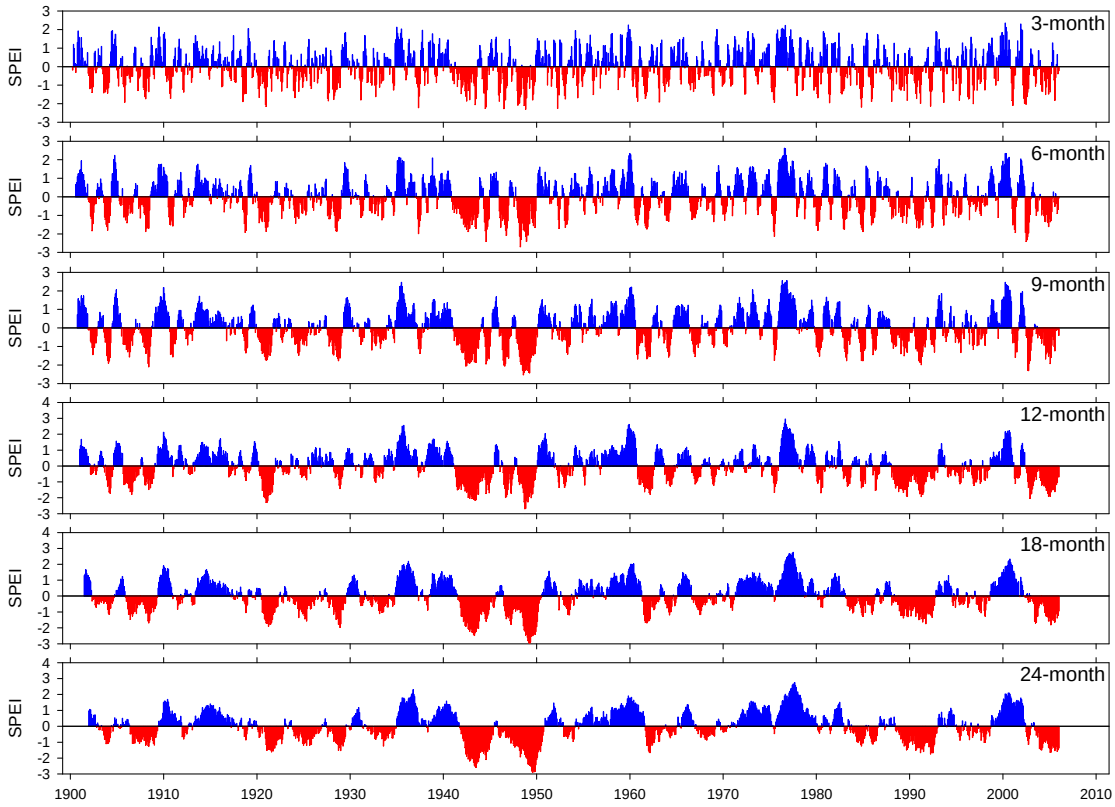

Figure S9. Example of drought evolution on different time scales as assessed by the SPEI. The series represents the evolution of the SPEI at 46.5°N, 8°E. Dry (negative SPEI values) and humid (positive SPEI values) periods are represented by red and blue bars, respectively.

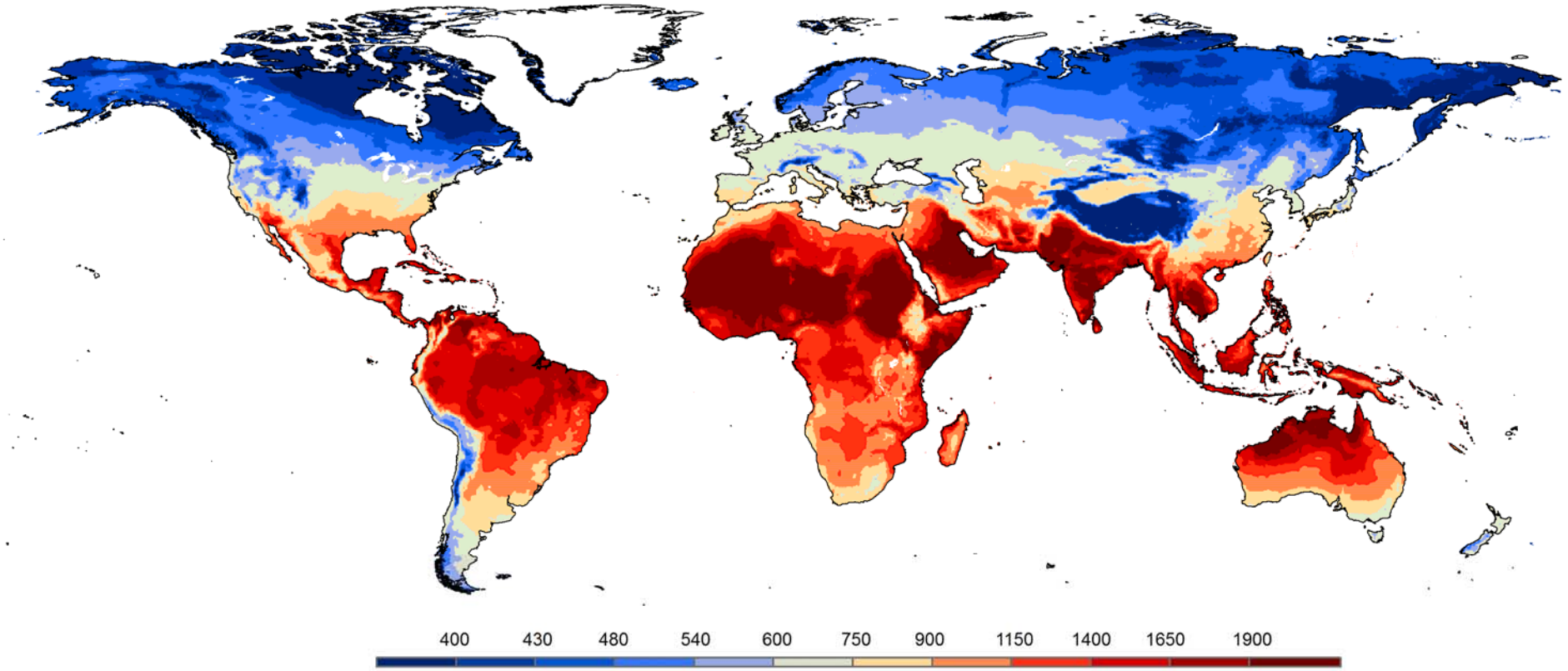

Figure S10. Spatial distribution of the average (1970-2000) potential evapotranspiration (PET) following the Thornthwaite's method.

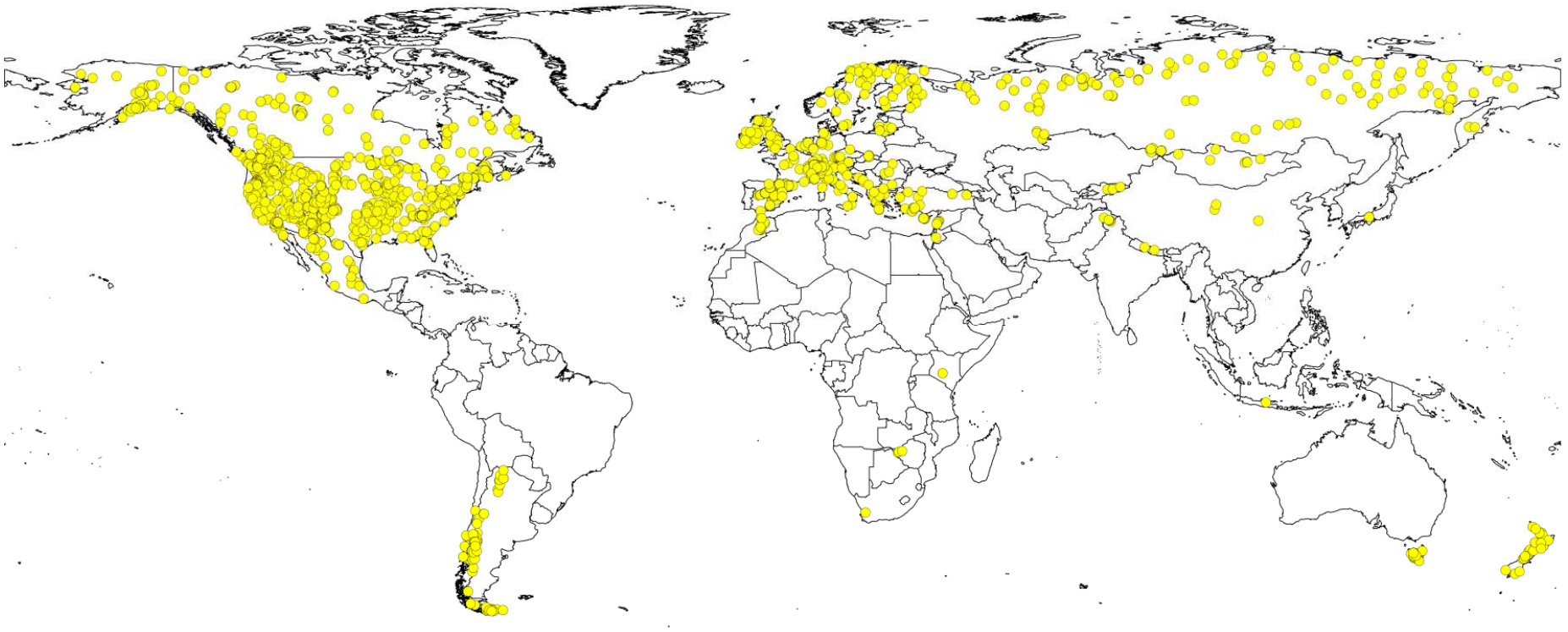

Figure S11. Spatial distribution of the tree-ring width series used in this study

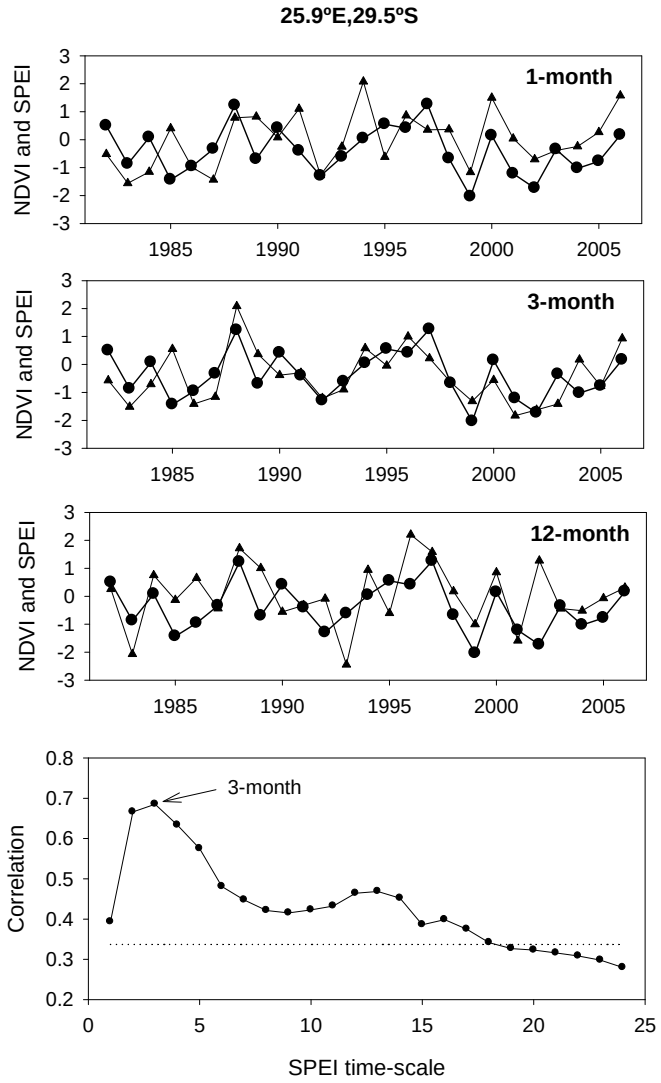

Figure S12: Evolution of standardized GIMMS-NDVI and 1-, 3- and 12-month SPEI in March in a warm temperate thorn scrub in South Africa (25.9ºE, 25.9ºS). The correlation between the NDVI (circles) series and the 1- to 24-SPEI (triangles) timescales is shown in the lower panel. Dotted line shows the threshold for statistically significant correlations.

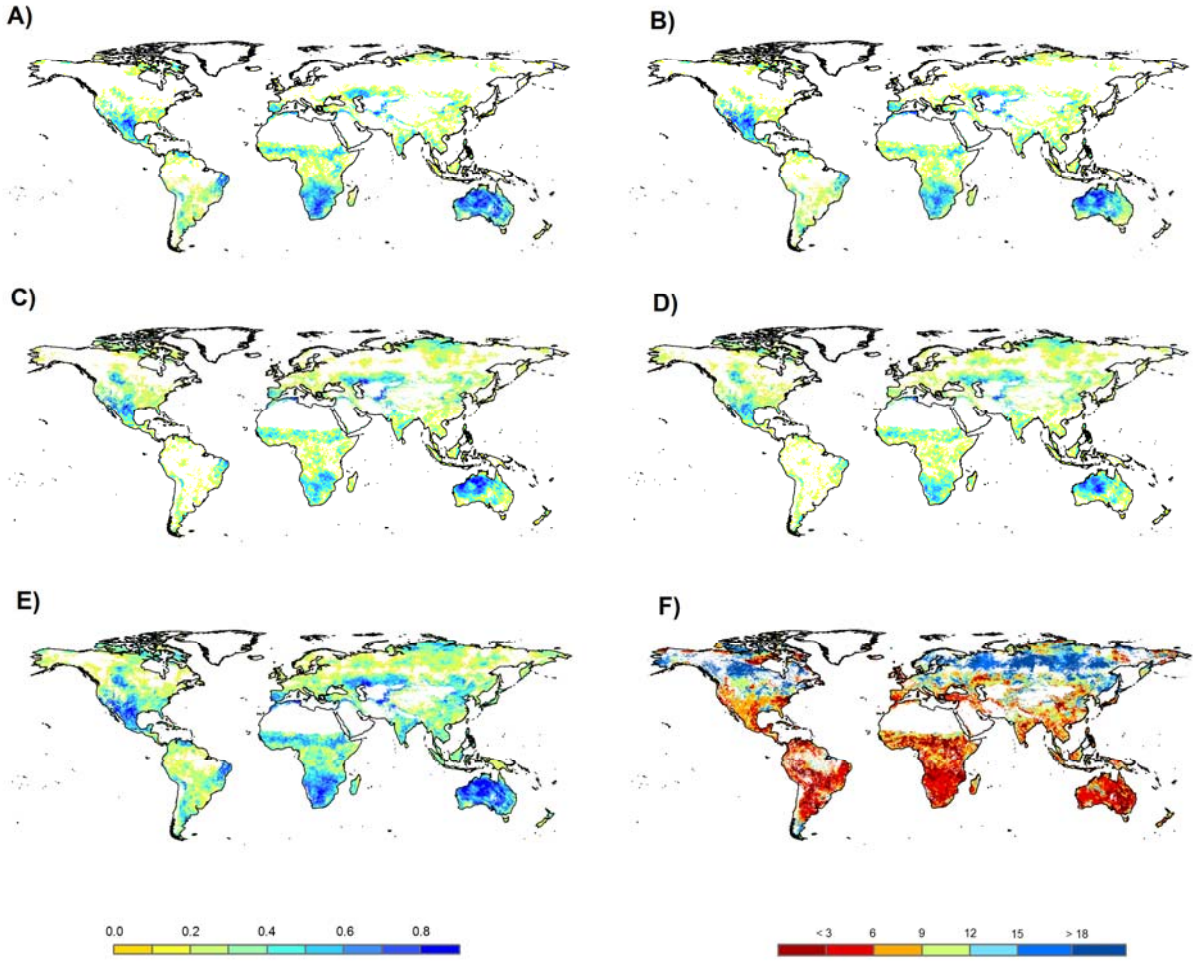

Figure S13. Spatial distribution of the May GIMMS-NDVI/SPEI correlations at the time scales of **A)** 3-, **B)** 6-, **C)** 12- and **D)** 18-months; **E)** maximum correlation found at time scales from 1 to 24 months and **F)** SPEI time scale (in months) at which the maximum correlation is found.

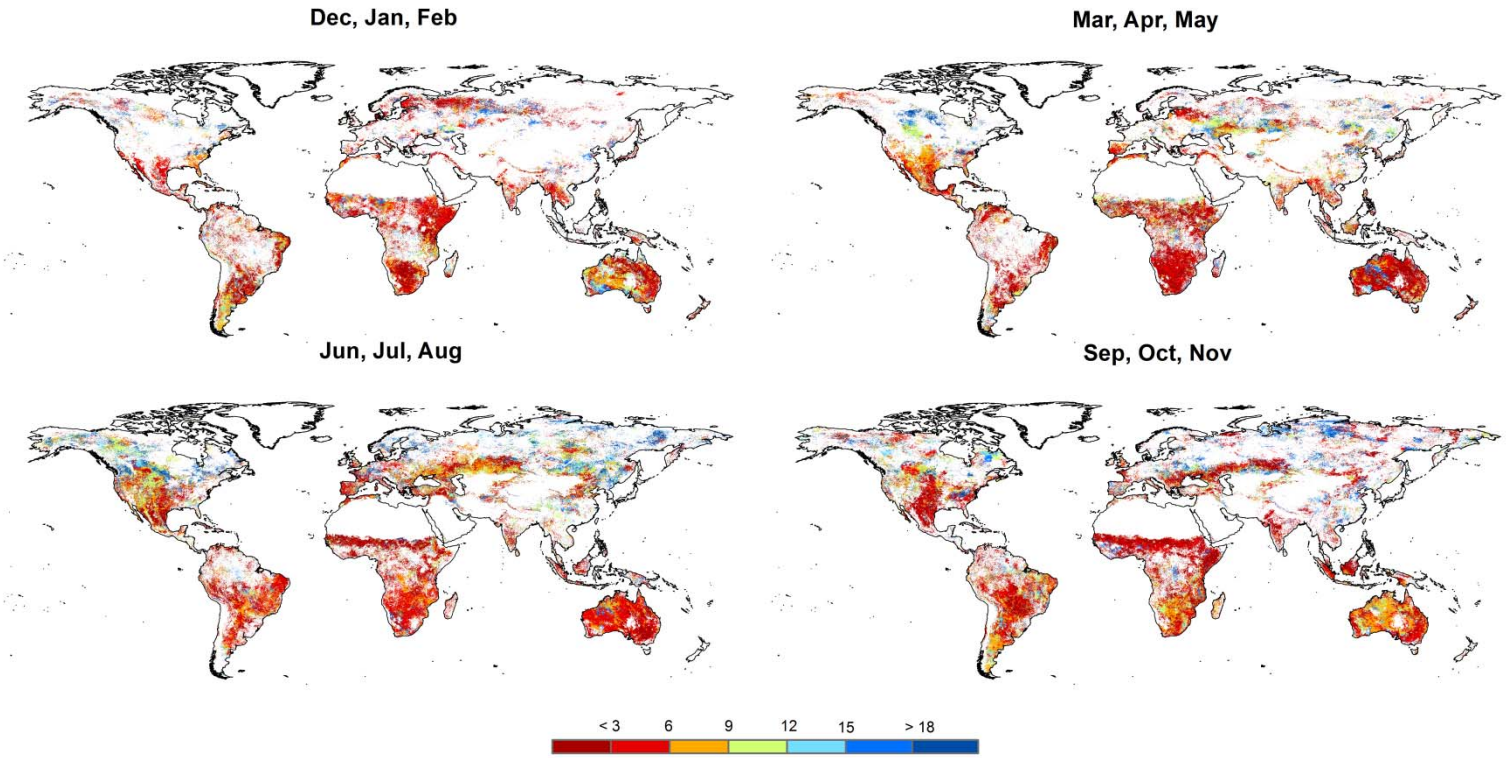

Figure S14. SPEI time scale (in months) at which the maximum seasonal correlation between SPEI and GIMMS-NDVI is found. Areas with no significant correlations are depicted in white. Desert and ice areas are masked and not included in the analysis.

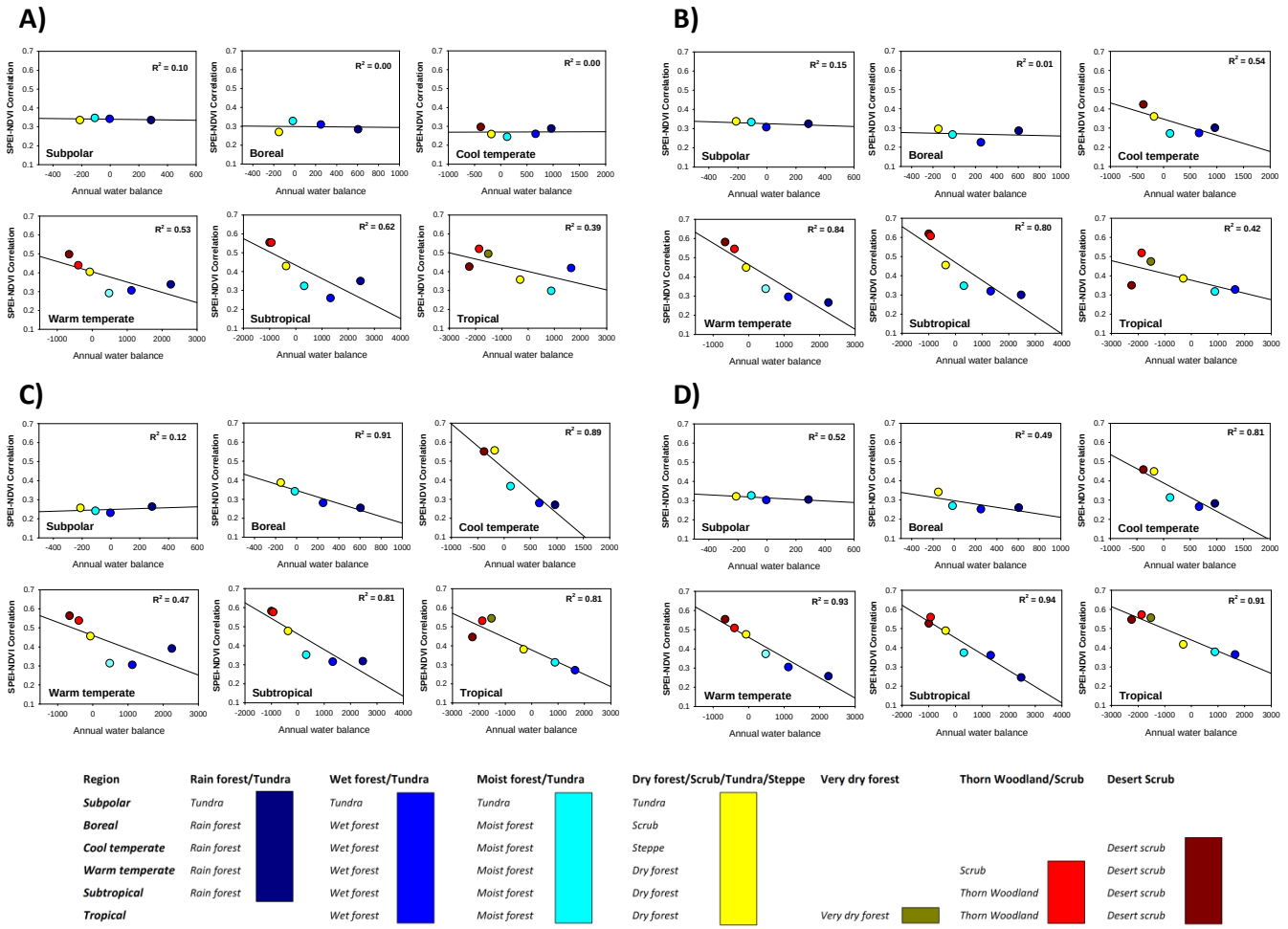

Figure S15. Relationships between SPEI/GIMMS-NDVI maximum Pearson correlation coefficients and the annual water balance across eco-regions. **A)** Dec, Jan, Feb; **B)** Mar, Apr, May; **C)** Jun, Jul, Aug; **D)** Sep, Oct, Nov. The biomes are grouped according to six eco-regions: Subpolar, Boreal, Cool temperate, Warm temperate, Subtropical and Tropical. All the biomes are represented by the same symbol (circle).

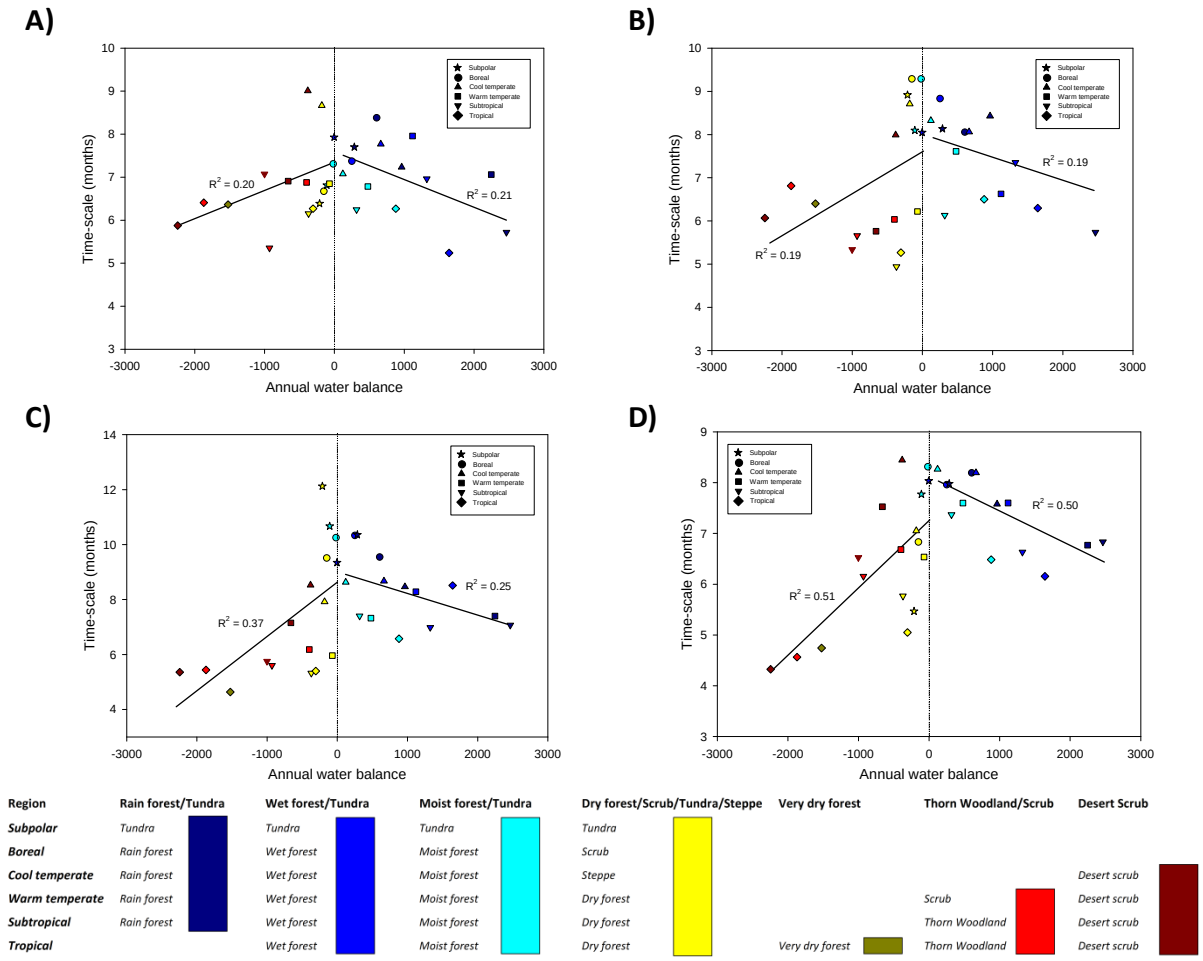

Figure S16. Seasonal relationships between the average SPEI time scales at which the maximum SPEI/GIMMS-NDVI correlation is found and the average annual water balance across eco-regions. **A)** Dec, Jan, Feb; **B)** Mar, Apr, May; **C)** Jun, Jul, Aug; **D)** Sep, Oct, Nov. The biomes are grouped according to the six existing eco-regions: Subpolar, Boreal, Cool temperate, Warm temperate, Subtropical and Tropical. Colors represent the different biomes of each one of the six eco-regions in the four plots and the symbols represent the different eco-regions.

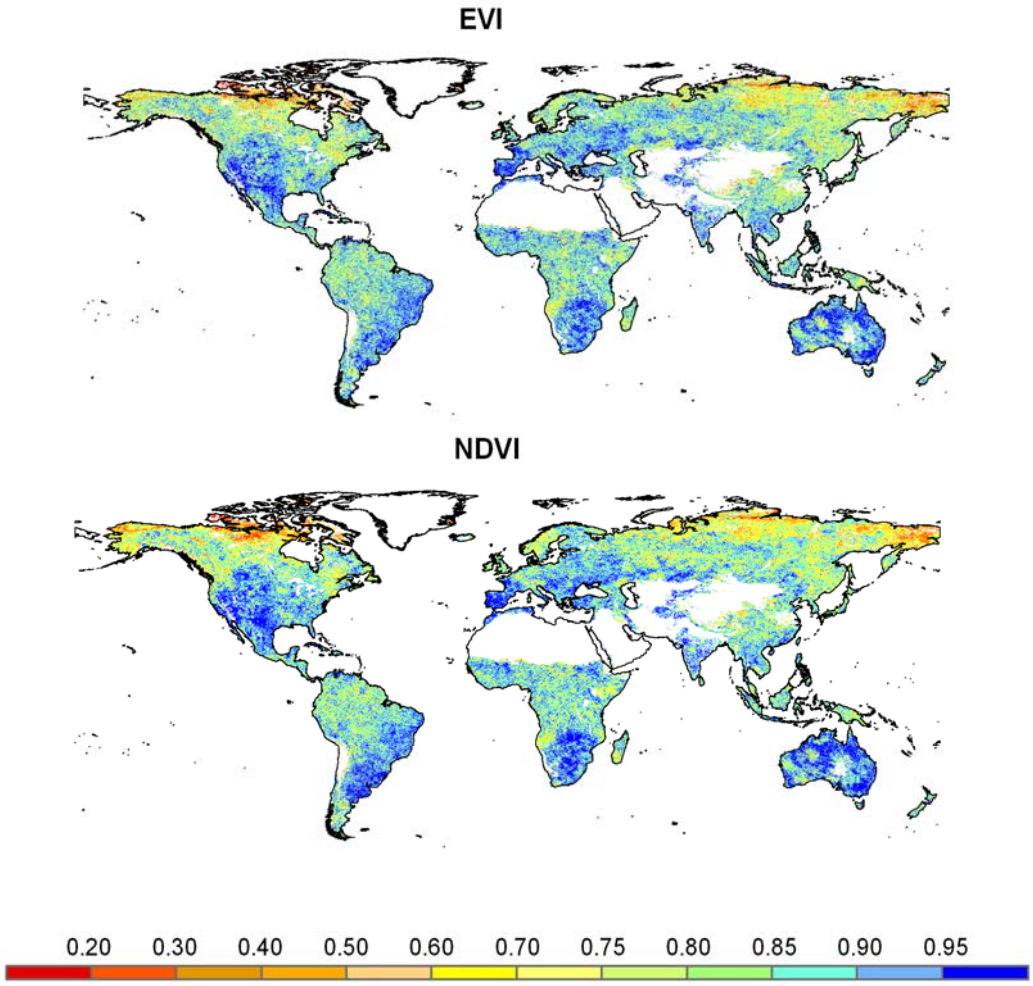

Figure S17. Spatial distribution of the correlations (Pearson coefficient, *r*) between SPEI and MODIS-EVI AND -NDVI for the period 2001-2009. The values represent the maximum correlation recorded for each pixel, independently of the month of the year and the SPEI time scale. Desert and ice areas are masked and not included in the analyses.

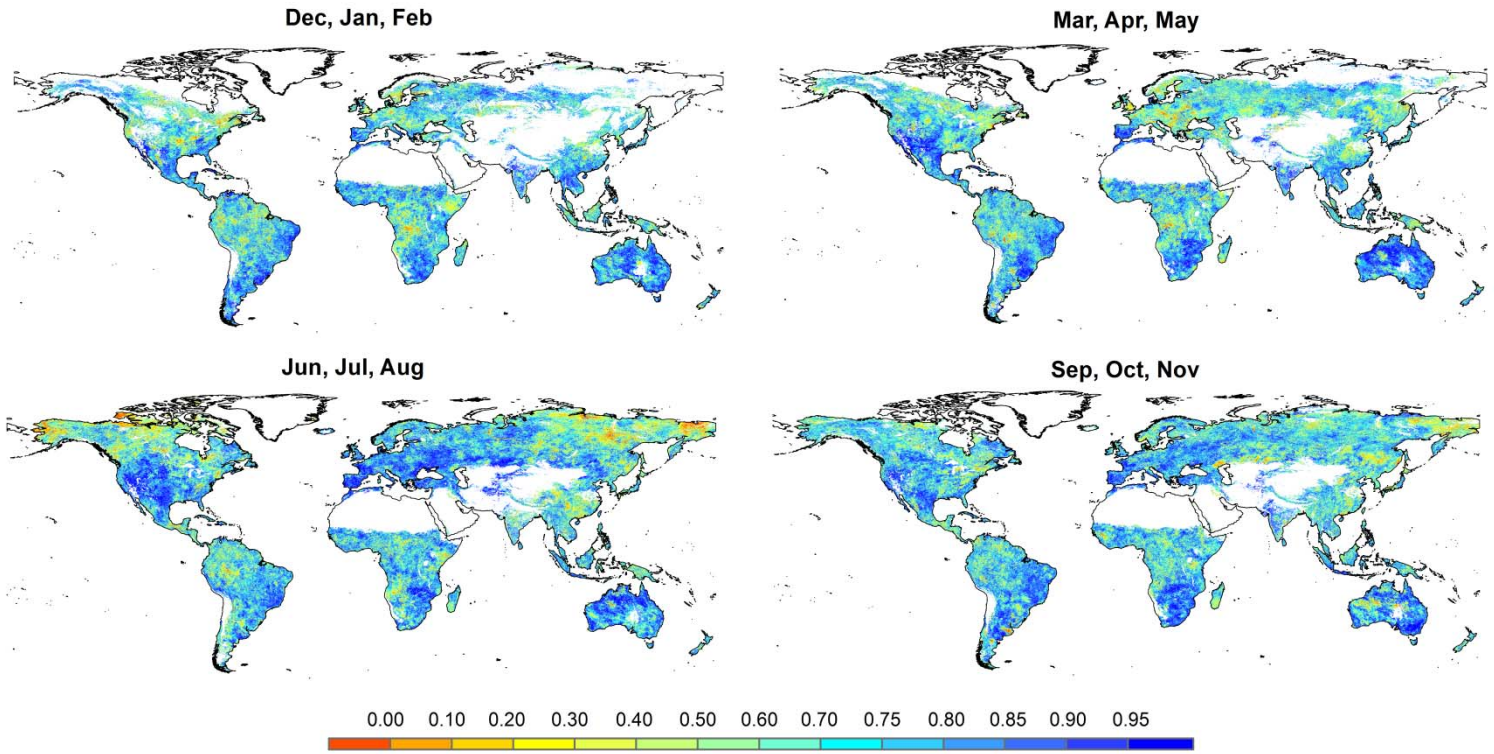

Figure S18. Spatial distribution of the seasonal correlations (Pearson coefficient, *r*) between SPEI and MODIS-EVI for the period 2001-2009. The values represent the maximum correlation recorded for each pixel, independently of the month of the year and the SPEI time scale. Desert and ice areas are masked and not included in the analysis.

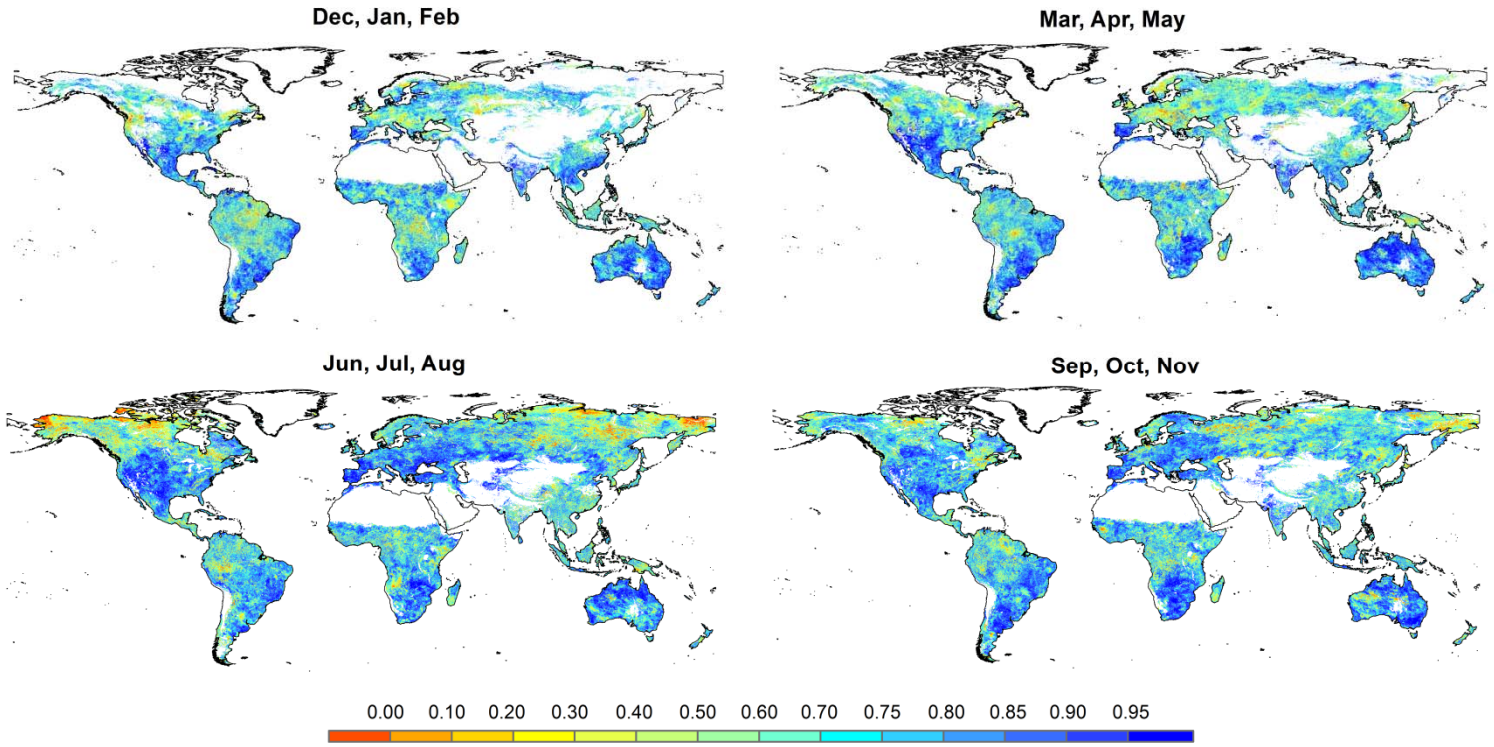

Figure S19. Spatial distribution of the seasonal correlations (Pearson coefficient, *r*) between SPEI and MODIS-NDVI for the period 2001-2009. The values represent the maximum correlation recorded for each pixel, independently of the month of the year and the SPEI time scale. Desert and ice areas are masked and not included in the analysis.

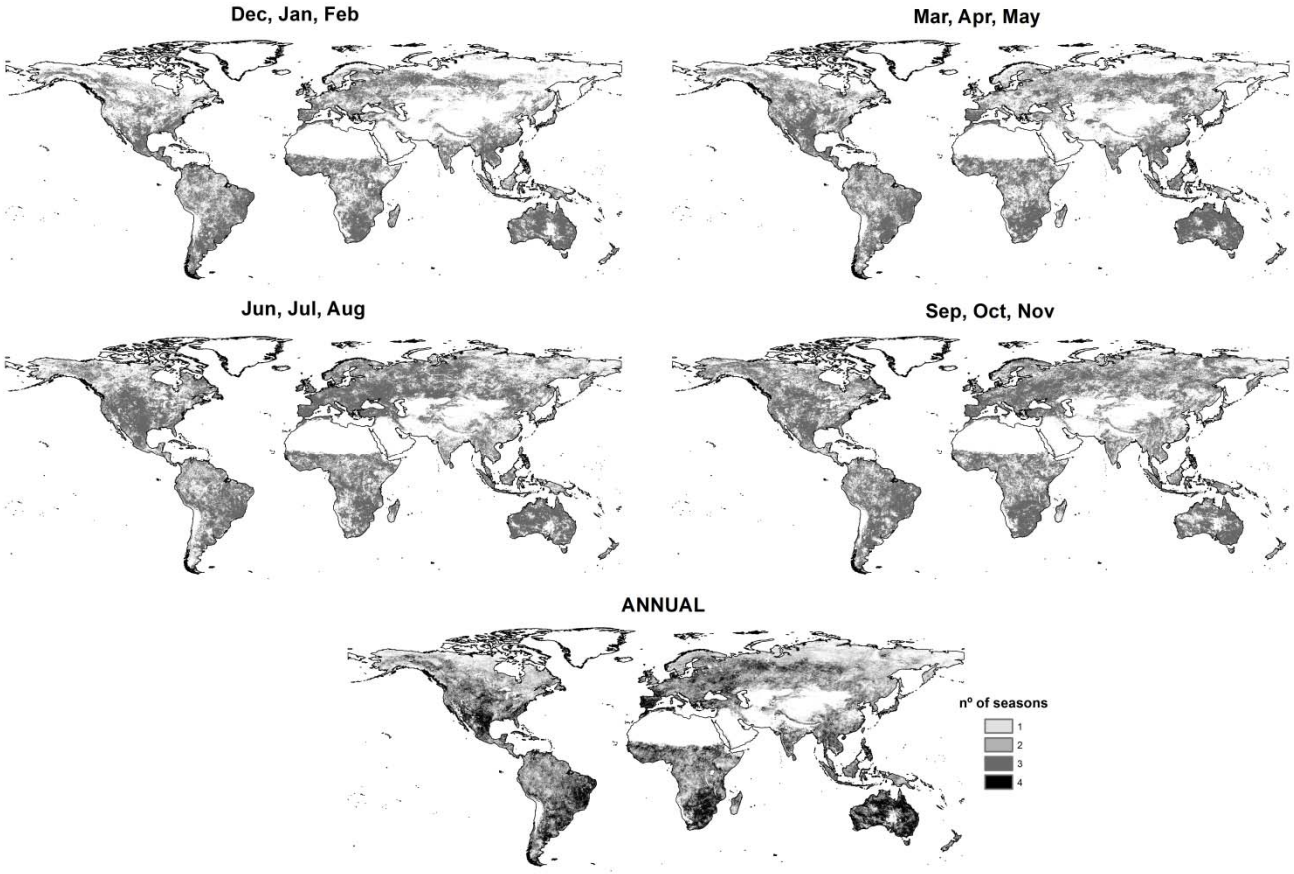

Figure S20. Areas with statistically significant Pearson correlation coefficients ($\alpha < 0.05$) between the SPEI and the MODIS-EVI for each season and the whole year. The legend of the lowermost annual map indicates the number of seasons in which significant correlations were obtained.

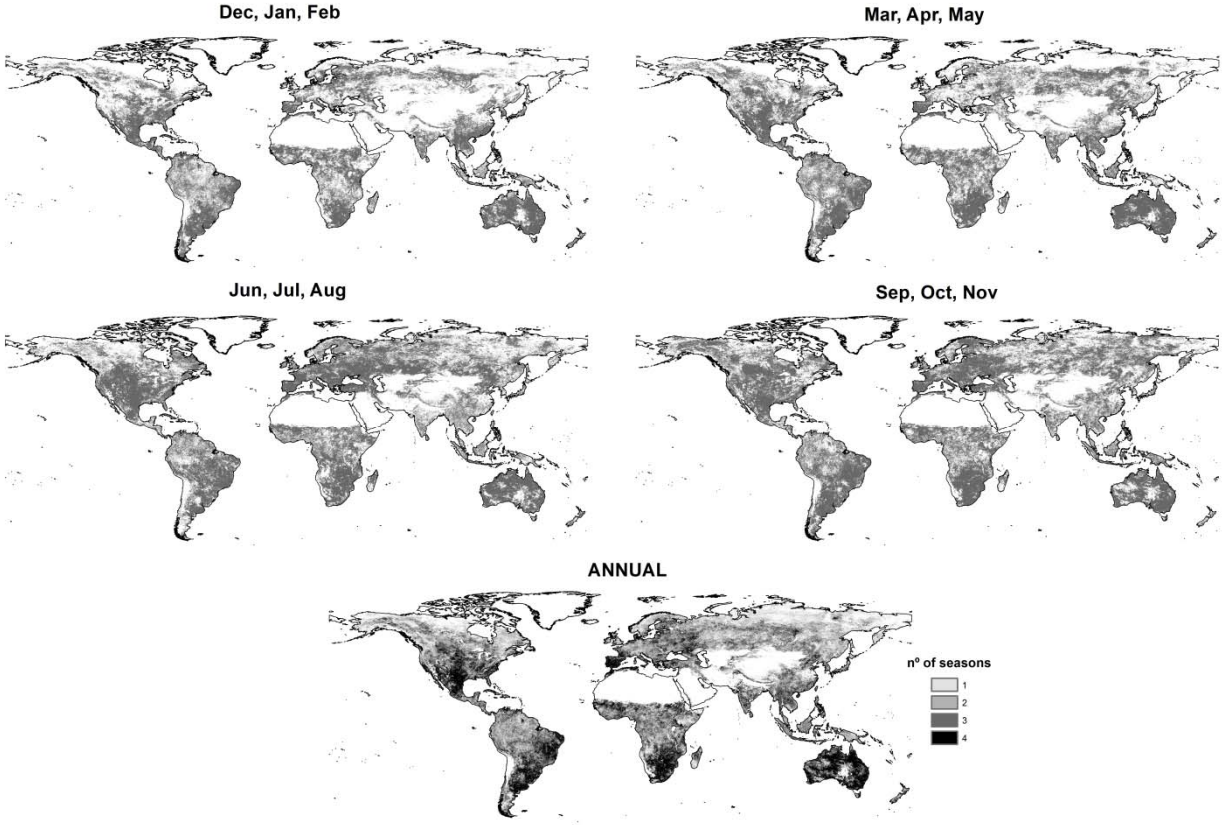

Figure S21. Areas with statistically significant Pearson correlation coefficients ($\alpha < 0.05$) between the SPEI and the MODIS-NDVI for each season and the whole year. The legend of the lowermost annual map indicates the number of seasons in which significant correlations were obtained.

A)

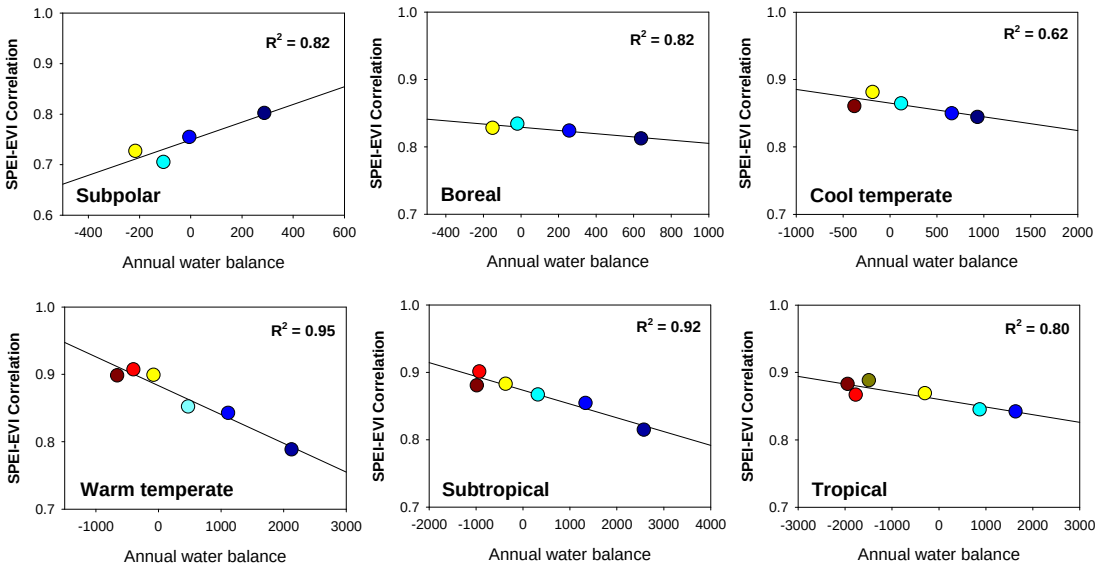

B)

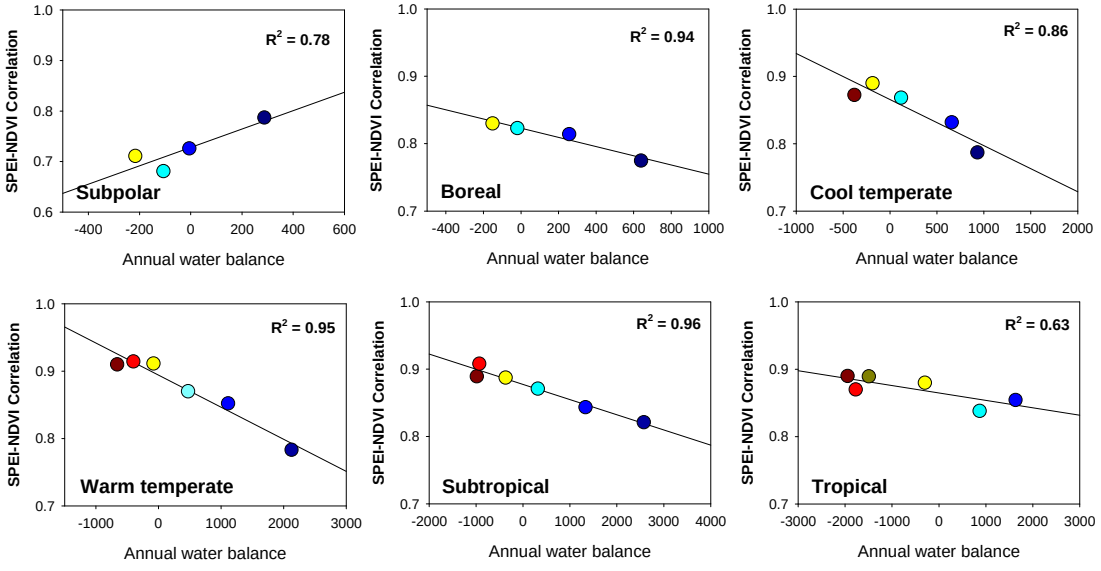

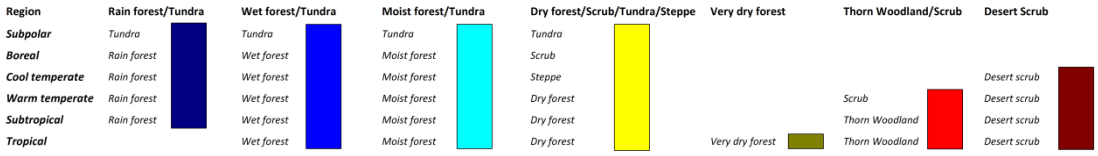

Figure S22. Relationship between **A)** SPEI/MODIS-EVI and **B)** SPEI/MODIS-NDVI maximum Pearson correlation coefficients and the annual water balance across eco-regions. The biomes are grouped in six eco-regions: Subpolar, Boreal, Cool temperate, Warm temperate, Subtropical and Tropical. All the biomes are represented by the same symbol (circle).

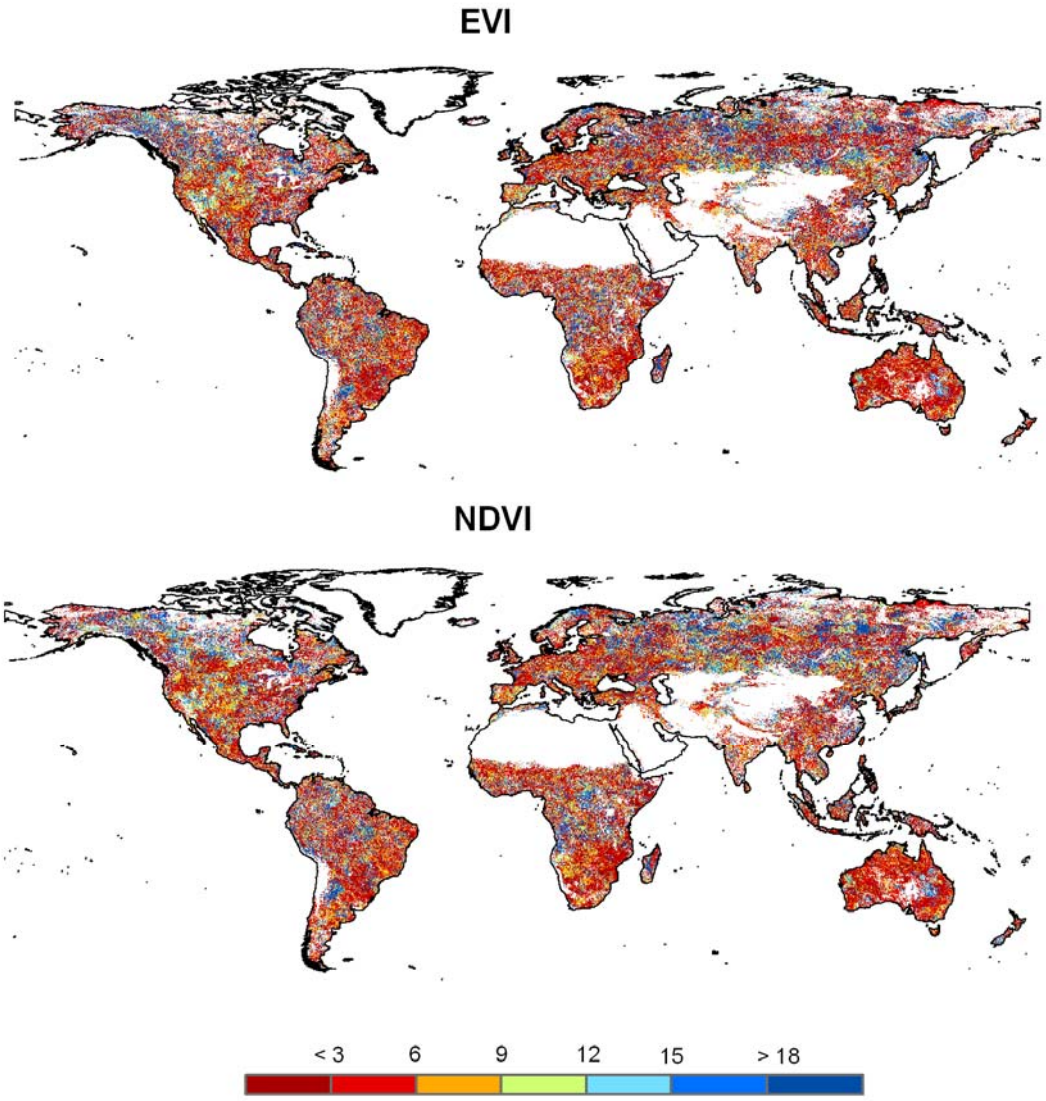

Figure S23. SPEI time scale (in months) at which the maximum correlation between SPEI and MODIS-EVI and MODIS-NDVI is found. Areas with no significant correlations are depicted in white. Desert and ice areas are masked and not included in the analyses.

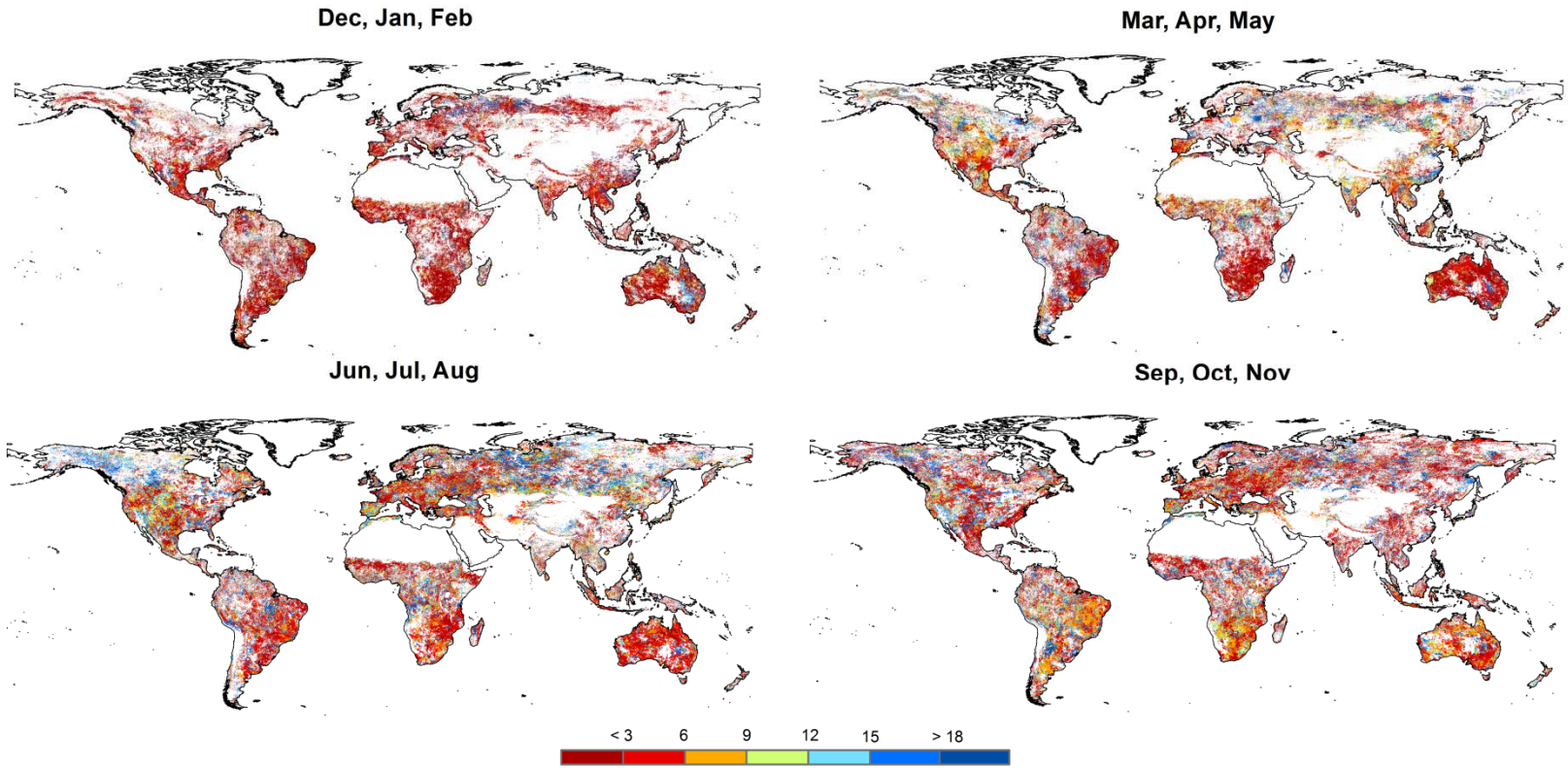

Figure S24. SPEI time scale (in months) at which the maximum seasonal correlation between SPEI and MODIS-EVI is found. Areas with no significant correlations are depicted in white. Desert and ice areas are masked and not included in the analyses.

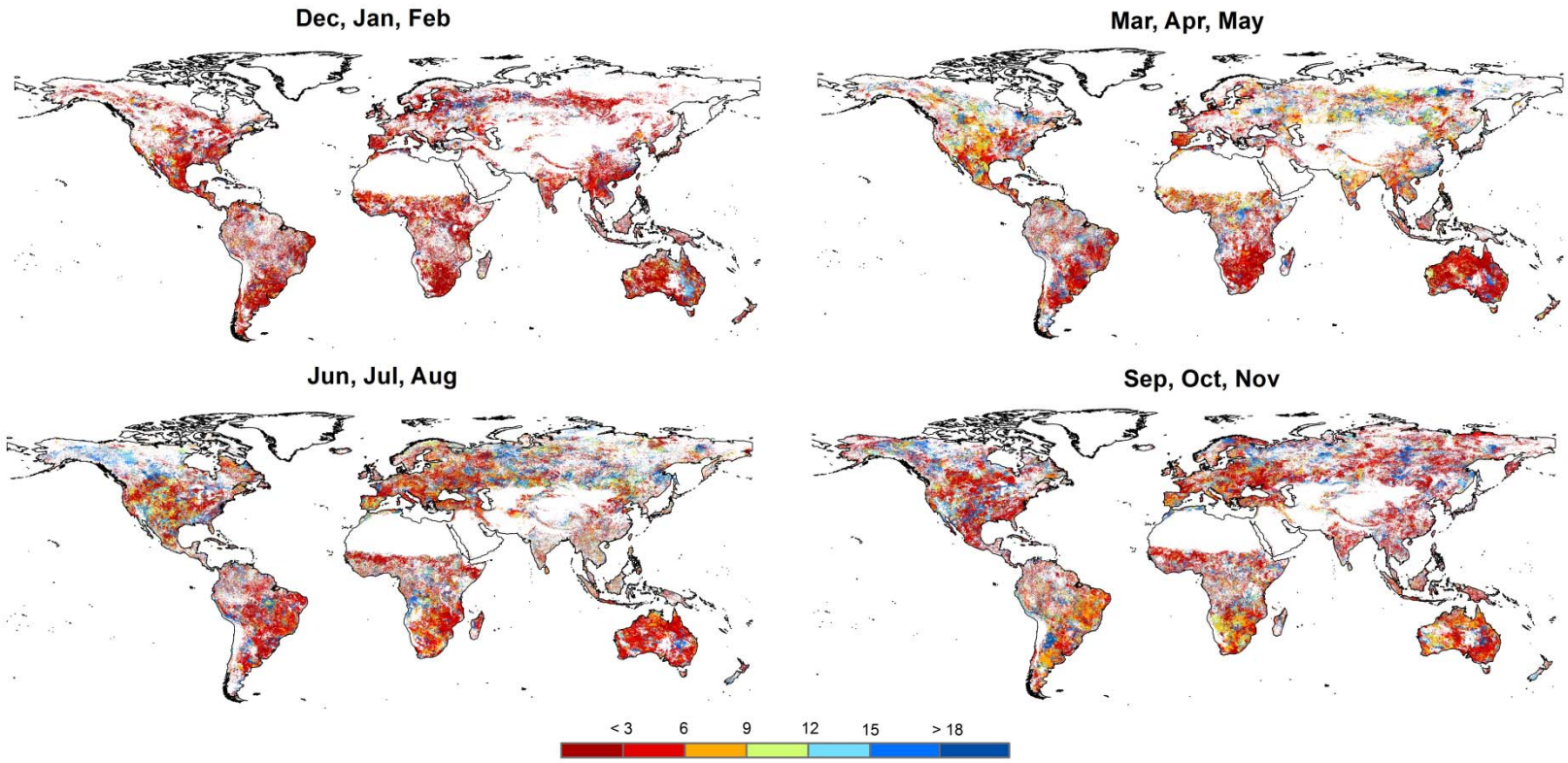

Figure S25. SPEI time scale (in moths) at which the maximum seasonal correlation between SPEI and MODIS-NDVI is found. Areas with no significant correlations are depicted in white. Desert and ice areas are masked and not included in the analysis.

5. Supplemental references

[S1]Heim RR (2002) A review of twentieth-century drought indices used in the United States. *Bulletin of the American Meteorological Society* 83: 1149-1165.

[S2]Keyantash J, Dracup J (2002) The quantification of drought: an evaluation of drought indices. *Bulletin of the American Meteorological Society* 83: 1167-1180.

[S3]Mishra AK, Singh VP (2010) A review of drought concepts. *Journal of Hydrology* 391: 202–216.

[S4]Sivakumar MVK, Motha RP, Wilhite DA, Wood DA (2010) Agricultural Drought Indices: Proceedings of an Expert Meeting, 2–4 June 2010, Murcia, Spain, 219 pp., World Meteorol. Org., Geneva, Switzerland.

[S5]Palmer WC (1965) *Meteorological droughts.* U.S. Department of Commerce Weather Bureau Research Paper 45, 58 pp.

[S6]McKee TBN, Doesken J, Kleist J (1993) The relationship of drought frecuency and duration to time scales. *Eight Conf. On Applied Climatology.* Anaheim, CA, Amer. Meteor. Soc. 179-184.

[S7]Guttman NB (1998) Comparing the Palmer drought index and the Standardized Precipitation Index. *Journal of the American Water Resources Association* 34: 113-121.

[S8]Hayes M, Wilhite DA, Svoboda M, Vanyarkho O (1999) Monitoring the 1996 drought using the Standardized Precipitation Index. *Bulletin of the American Meteorological Society* 80: 429-438.

[S9]Hayes M, Svoboda M, Wall N, Widhalm M (2011) The Lincoln Declaration on Drought Indices: Universal Meteorological Drought Index recommended, *Bulletin of the American Meteorological Society* 92: 485–488.

[S10]Szalai S, Szinell CS, Zoboki J (2000) Drought monitoring in Hungary. In *Early warning systems for drought preparedness and drought management.* World Meteorological Organization. Lisboa: 182-199.

[S11]Vicente-Serrano SM, López-Moreno JI (2005) Hydrological response to different time scales of climatological drought: an evaluation of the standardized precipitation index in a mountainous Mediterranean basin. *Hydrology and Earth System Sciences* 9: 523-533.

[S12]Khan S, Gabriel HF, Rana T (2008) Standard precipitation index to track drought and assess impact of rainfall on watertables in irrigation areas. *Irrigation and Drainage Systems* 22: 159-177.

[S13]Fiorillo F, Guadagno FM (2010) Karst spring discharges analysis in relation to drought periods, using the SPI. *Water Resources Management* 24: 1867-1884.

[S14]Vicente-Serrano SM, Cuadrat JM, Romo A (2006) Early prediction of crop productions using drought indices at different time scales and remote sensing data: application in the Ebro valley (North-east Spain). *International Journal of Remote Sensing* 27: 511-518.

[S15]Quiring SM, Ganesh S (2010) Evaluating the utility of the Vegetation Condition Index (VCI) for monitoring meteorological drought in Texas. *Agricultural and Forest Meteorology* 150: 330-339.

[S16]Abramopoulos F, Rosenzweig C, Choudhury B (1998) Improved ground hydrology calculations for global climate models (GCMs): Soil water movement and evapotranspiration. *Journal of Climate* 1: 921–941.

[S17]Williams AP, Xu Ch, McDowell NG (2011) Who is the new sheriff in town regulating boreal forest growth?. *Environmental Research letters* 6: doi: 10.1088/1748-9326/6/4/041004.

[S18]Martínez-Villalta J, López BC, Adell N, Badiella L, Ninyerola M (2008) Twentieth century increase of Scots pine radial growth in NE Spain shows strong climate interactions. *Global Change Biology* 14: 2868–2881.

[S19]Vicente-Serrano SM, Lasanta T, Gracia C (2010) Aridification determines changes in leaf activity in Pinus halepensis forests under semiarid Mediterranean climate conditions. *Agricultural and Forest Meteorology* 150: 614-628.

[S20]McGuire AD, et al. (2010) Vulnerability of white spruvce tree growth in interior Alaska in response to climate variability: ddendrochronological, demographic, and experimental perspectives. *Canadian Journal of Forest Research,* 40: 1197-1209.

[S21]Linares JC, Camarero JJ (2011) From pattern to process: linking intrinsic water-use efficiency to drought-induced forest decline. *Global Change Biology* 18: 1000-1015.

[S22]Rebetez M, et al. (2006) Heat and drought 2003 in Europe: A climate synthesis. *Annals of Forest Science* 63: 569-577.

[S23]Barriopedro D, Fischer EM, Luterbacher J, Trigo RM, García-Herrera R (2011) The hot summer of 2010: Redrawing the temperature record map of Europe. *Science* 332: 220-224.

[S24]Lobell DB, Schlenker W, Costa-Roberts J (2011) Climate trends and global crop production since 1980. *Science* 29: 616-620.

[S25]Vicente-Serrano SM, Beguería S, López-Moreno JI, Angulo M, El Kenawy A (2010) A new global 0.5° gridded dataset (1901-2006) of a multiscalar drought index: comparison with current drought index datasets based on the Palmer Drought Severity Index. *Journal of Hydrometeorology* 11: 1033–1043.

[S26]Köppen W (1936) Das Geographische System der Klimate. In Köppen, C.W. & Geiger, R., eds., Handbuch der Klimatologie ,vol. 3. Berlin:Gebrüder Bornträger.

[S27]Thornthwaite CW (1948) An approach toward a rational classification of climate. *Geographical Review* 38: 55-94.

[S28]Budyko MI (1974) *Climate and life*, Academic, New York.

[S29]UNEP (1992) World Atlas of Desertification. Edward Arnold. London.

[S30]Knipling EB (1970) Physical and physiological basis for the reflectance of visible and near-infrared radiation from vegetation. *Remote Sensing of Environment* 1: 155-159.

[S31]McVicar TR, Jupp DLB (1998) The current and potential operational uses of remote sensing to aid decisions on drought exceptional circumstances in Australia: a review. *Agricultural Systems* 57: 399-468.

[S32]Tucker CJ (1979) Red and photographic infrared linear combinations for monitoring vegetation. *Remote Sensing of Environment* 8: 127-150.

[S33]Bannari A, Morin D, Bonn F, Huete AR (1995) A review of vegetation indices. *Remote Sensing Reviews* 13: 95–120.

[S34]Baret F, Guyot G (1991) Potential and limits of vegetation indices for LAI and APAR assessment. *Remote Sensing of Environment* 35: 161–173.

[S35]Rouse JW, et al. (1974) *Monitoring the vernal advancement and retrogradation (greenwave effect) of natural vegetation.* NASA/GSFC type III Final Report, Greenbelt, MD.

[S36]Curran PJ (1980) Multispectral remote sensing of vegetation amount. *Progress in Physical Geography* 4: 315-341.

[S37]Holben BN, Tucker CJ, Fan C-J (1980) Spectral assessment of soybean leaf area and lear biomass.

Photogrammetric Engineering & Remote Sensing 46: 651-656.

[S38]Tucker CJ, Vanpraet CL, Sharman MJ, Van Ittersum G (1985) satellite remote sensing of total herbaceous biomass production in the Senegalese Sahel: 1980-1984. *Remote Senisng of Environment* 17: 233-249.

[S39]Myneni RB, et al (1995) Optical remote sensing of vegetation: modelling, caveats and algortihms. *Remote Sensing of Environment* 51: 169-188.

[S40]Hatfield JL, Asrar G, Kanemasu ET (1984) Intercepted photosynthetically active radiation estimated by spectral reflectance. *Remote Sensing of Environment* 14: 65-75.

[S41]Gallo KP, Daughtry CST, Bauer ME (1985) Spectral estimation of absorbed photosinthetically active radiation in corn canopies. *Remote Sensing of Environment* 17: 221-232.

[S42]Carlson TN, Perry EM, Schumugge TJ (1990) Remote estimation of soil moisture availability and fractional vegetation cover for agricultural fields. *Agricultural and Forest Meteorology* 52: 45-69.

[S43]Spanner MA, Pierce LL, Running SW, Peterson DL (1990) The seasonality of AVHRR data of temperate coniferous forests: relationship with leaf area index. *Remote Sensing of Environment* 33: 97-112.

[S44]Carlson TN, Ripley DA (1997) On the relation between NDVI, fractional vegetation cover, and leaf area index. *Remote Sensing of Environment* 62: 241-252.

[S45]Tucker CJ, Holben BN, Elgin JH, McMurtrey JE (1981) Remote Sensing of total dry matter accumulation in winter wheat. *Remote Sensing of Environment* 11: 171-189.

[S46]Tucker CJ, Vanpraet C, Boerwinkel E, Gaton A. (1981) Satellite remote sensing of total dry matter accummulation in winter wheat. *Remote Sensing of Environment* 11: 171-189.

[S47]Cihlar J, StLaurent L, Dyer JA (1991) The relation between normalized difference vegetation index and ecological variables. *Remote Sensing of Environment* 35: 279-298.

[S48]Gutman GG (1991) Vegetation indices from AVHRR. An update and future prospects. *Remote Sensing of Environment* 35: 121-136.

[S49]Asner GP, Alencar A (2010) Drought impacts on the Amazon forest: the remote sensing perspective. *New Phytologist* 187: 569-578.

[S50]Gutman GG (1990) Towards monitoring droughts from space. *Journal of Climate* 3: 282-295.

[S51]Che N, Price JC (1992) Survey of radiometric calibration results and method for visible and near infrared channels of NOAA –7, -9 and –11 AVHRRs. *Remote Sensing of Environment* 41: 19-27.

[S52]Schultz PA, Halpert MS (1995) Global analysis of the relationships among a vegetation index. Precipitation and land surface temperature. *International Journal of Remote Sensing* 16: 2755-2777.

[S53]Beck H, et al. (2011) Global evaluation of four AVHRR-NDVI data sets: Intercomparison and assessment against Landsat imagery. *Remote Sensing of Environment* 115: 2547-2563.

[S54]Justice DH, et al. (1998) The Moderate Resolution Imaging Spectroradiometer (MODIS): land remote sensing for global change research. *IEEE Transactions on Geoscience and Remote Sensing* 36: 1228–1249.

[S55] Huete A, et al. (2002) Overview of the radiometric and biophysical performance of the MODIS vegetation indices. *Remote Sensing of Environment* 83: 195-213.

[S56]Gao X, Huete AR, Ni W, Miura T (2000) Optical-biophysical relationships of vegetation spectra without background contamination. *Remote Sensing of Environment* 74: 609-620.

[S57] Didan K, Huete AH (2006) MODIS Vegetation Index Product Series Collection 5 Change Summary TBRS Lab., The University of Arizona June 29th, 2006. http://landqa2.nascom.nasa.gov/QA_WWW/forPage/MOD13_VI_C5_Changes_Document_06_28_06.pdf.

[S58]Grissino-Mayer HD, Fritts HC (1997) The International Tree-Ring Data Bank: an enhanced global database serving the global scientific community. *The Holocene* 7: 235-238.

[S59]Stokes MA, Smiley TL (1968) *An introduction to tree ring dating*. The University of Chicago Press, Chicago.

[S60]Holmes RL (1983) Computer-assisted quality control in tree-ring dating and measurement. *Tree-Ring Bulletin* 43: 69-78.

[S61]Brewer PW, Murphy D, Jansma E (2011) Tricycle: A Universal Conversion Tool For Digital Tree-Ring Data. *Tree-Ring Research* 67: 135-144.

[S62]Williams AP, et al. (2010) Forest responses to increasing aridity and warmth in the southwestern United States. *Proceedings of the National Academy of Sciences of the United States of America,* doi: 10.1073/pnas.0914211107.

[S63]Cook ER, Krusic PJ (2005) Program Arstan, a tree-ring standardization program based on detrending and autoregressive time series modeling, with interactive graphics. Tree-ring Laboratory Lamont Doherty Earth Observatory of Columbia University, Palisades, NY.

[S64]Murphy AH (1970) Predicted forage yields based on fall precipitation in California annual grasslands. *Journal of Range Management* 23: 363-365.

[S65]Passey HB, Hugie VK, Williams EW, Ball DE (1982) *Relationships between soil, plant community, and climate on rangelands of the Intermountain West.* U.S. Department of Agriculture, Technical Bulletin No. 1669.

[S66]Frichnecht NC, Harris LE (1968) *Grazing intensities and systems on crested wheatgrass in central Utah. Response of vegetation and cattle.* US Department of Agriculture, Bulletin 1388, Washington DC.

[S67]Blaisdell J (1958) *Seasonal development and yield of native plants on the upper Snake River Plain and their relation to certain climatic factors.* United States Department of Agriculture Technical Bulletin 1190.

[S68]Smoliak S (1986) Influence of climatic conditions on production of *Stipa Bouteloua* prairie over a 50-year period. *Journal of Range Management* 39: 100-103.

[S69]Cable DR (1975) Influence of Precipitation on Perennial Grass Production in the Semidesert Southwest. *Ecology* 56: 981-986.

[S70]Khumalo G, Holechek J (2005) Relationships between Chihuahuan desert perennial grass production and precipitation. *Rangeland Ecology & Management* 58: 239-246.

[S71]Andales AA, Derner JD, Ahuja JR, Hart RH (2006) Strategic and Tactical Prediction of Forage Production in Northern Mixed-Grass Prairie. *Rangeland Ecological Management* 59: 576–584.

[S72]Lauenroth WK, Sala OE (1992) Long-Term Forage Production of North American Shortgrass Steppe. *Ecological Applications* 2: 397-403.

[S73]Wight JP, Black AL (1979) range fertilization: plant response and water use. *Journal of Range Management* 32: 345-349.

[S74]Rogler GA, Haas HJ (1947) range production as related to soil moisture and precipitation on the northern Great plains. *Journal of the American Society of Agronomy* 38: 378-389.

[S75]Patton BD, Dong X, Nyren PE, Nyren A (2007) Effects of Grazing Intensity, Precipitation, and Temperature on Forage Production. *Rangeland Ecol Manage* 60: 656–665

[S76]Hulett GK, Tomanek GW (1968) Forage production on a clay upland range site in Western Kansas. *Journal of Range Management* 22: 270-276.

[S77]ORNL DAAC (2012) Net Primary Productivity (NPP) Data Sets. http://daac.ornl.gov/cgi-bin/dataset_lister.pl?p=13. Last access 10/04/2012.

[S78]Towne G, Owensby C (1984) Long term effects of annual burning at different dates in ungrazed kansas tallgrass prairie. *Journal of Range Management* 37*:* 392-397*.*

[S79]Bhattacharjee J, Haukos DA, Neaville J (2009) Influence of biotic and abiotic factors on annual aboveground biomass of an intermediate coastal marsh. *Wetlands* 29: 690-696.

[S80]Conner WH, Song B, Williams TM, Vernon JT (2011) Long-term tree productivity of a South Carolina coastal plain forest across a hydrology gradient. *Journal of Plant Ecology* 4: 67-76.

[S81]Jobbagy EG, Sala OE (2000) Controls of grass and shrub aboveground production in the Patagonian steppe. *Ecological Applications* 10: 541-549.

[S82]O'Connor TG, Haines LM, Snyman HA (2001) Influence of precipitation and species composition on phytomass of a semi-arid African grassland. *Journal of Ecology* 89: 850-860.

[S83]Tadmor NH, Eyal E, Benjamin RW (1974) Plant and sheep production on semiarid annual grassland in Israel. *Journal of Range Management* 27: 427-432.

[S84]Henkin Z, Seligman NG, Noy-Meir I (2010) Long-term productivity of Mediterranean herbaceous vegetation after a single phosphorus application. *Journal of Vegetation Science* 21: 979–991.

[S85]Bai Y, Han X, Wu J, Chen Z (2004) Ecosystem stability and compensatory effects in the Inner Mongolia grassland. *Nature* 431: 181-184.

[S86]Bentley JR, Talbot MW (1951) *Efficient use of annual plants on cattle ranges in the California foothills.* United States Department of Agriculture. Circular nº 870. Washington, D.C.

[S87]Fabrichon V (1997) Réaction de peuplements forestiers tropicaux a des interventions sylvicoles. *Bois et forêts del Tropiques* 254: 5-24.

[S88]Manokaran N, Kochummen KM (1987) Recruitment, Growth and Mortality of Tree Species in a Lowland Dipterocarp Forest in Peninsular. *Journal of Tropical Ecology* 3: 315-330.

[S89]Clark DA, Brown S, Kicklighter DW, Chambers JQ (2001) Measuring net primary production in forests: concept and field methods. *Ecological Applications* 11: 356–370.

[S90]Zweifel R, et al. (2010) Link between continuous stem radius changes and net ecosystem productivity of a subalpine Norway spruce forest in the Swiss Alps. *New Phytologist* 187: 819–830.

[S91]Etzold S, Ruehr NK, Zweifel R, Dobbertin M, Zingg A (2011) The carbon balance of two contrasting mountain forest ecosystems in Switzerland: similar annual trends, but seasonal differences. *Ecosystems* 14: 1289–1309.